11294–11311 *Nucleic Acids Research, 2021, Vol. 49, No. 19* *Published online 22 September 2021*
https://doi.org/10.1093/nar/gkab834

ZNF598 co-translationally titrates poly(GR) protein implicated in the pathogenesis of *C9ORF72*-associated ALS/FTD

Jumin Park†, Jongbo Lee†, Ji-hyung Kim, Jongbin Lee, Heeju Park and Chunghun Lim*

Department of Biological Sciences, Ulsan National Institute of Science and Technology, Ulsan 44919, Republic of Korea

Received August 24, 2021; Editorial Decision September 07, 2021; Accepted September 09, 2021

ABSTRACT

***C9ORF72*-derived dipeptide repeat proteins have emerged as the pathogenic cause of neurodegeneration in amyotrophic lateral sclerosis and frontotemporal dementia (C9-ALS/FTD). However, the mechanisms underlying their expression are not fully understood. Here, we demonstrate that ZNF598, the rate-limiting factor for ribosome-associated quality control (RQC), co-translationally titrates the expression of *C9ORF72*-derived poly(GR) protein. A *Drosophila* genetic screen identified key RQC factors as potent modifiers of poly(GR)-induced neurodegeneration. ZNF598 overexpression in human neuroblastoma cells inhibited the nuclear accumulation of poly(GR) protein and decreased its cytotoxicity, whereas *ZNF598* deletion had opposing effects. Poly(GR)-encoding sequences in the reporter RNAs caused translational stalling and generated ribosome-associated translation products, sharing molecular signatures with canonical RQC substrates. Furthermore, ZNF598 and listerin 1, the RQC E3 ubiquitin-protein ligase, promoted poly(GR) degradation via the ubiquitin-proteasome pathway. An ALS-relevant ZNF598^{R69C} mutant displayed loss-of-function effects on poly(GR) expression, as well as on general RQC. Moreover, RQC function was impaired in C9-ALS patient-derived neurons, whereas lentiviral overexpression of ZNF598 lowered their poly(GR) expression and suppressed proapoptotic caspase-3 activation. Taken together, we propose that an adaptive nature of the RQC-relevant ZNF598 activity allows the co-translational surveillance to cope with the atypical expression of pathogenic poly(GR) protein, thereby acquiring a neuroprotective function in C9-ALS/FTD.**

INTRODUCTION

Amyotrophic lateral sclerosis (ALS) is a fatal motor neuron disease that manifests as progressive motor dysfunction and respiratory failure. The characteristic symptoms associated with ALS are distinct from the behavioral, linguistic and cognitive deficits observed in frontotemporal dementia (FTD) patients (1,2). Nonetheless, these two neurodegenerative disorders share *C9ORF72* as a major genetic contributor to their development (3–5). The wild-type *C9ORF72* locus includes fewer than 20–30 tandem repeats of the GGGGCC hexanucleotide in the first intron, whereas this repeat is expanded to hundreds of copies in the ALS/FTD-associated *C9ORF72* locus. Pathogenic mutations may cause loss of *C9ORF72* function or gain of RNA toxicity (6,7). In addition, bidirectional transcription and repeat-associated non-AUG–initiated (RAN) translation from mutant loci lead to the production of a set of dipeptide repeat (DPR) proteins—poly(GR), poly(GA), poly(GP), poly(PR) and poly(PA)—in ALS/FTD neurons (8–10). Emerging evidence indicates that individual DPR proteins interact with distinct groups of factors and disrupt specific cellular functions, including causing the loss of nuclear integrity and nucleocytoplasmic transport (11–18). Accordingly, these effects are thought to collectively contribute to the molecular pathogenesis underlying *C9ORF72*-associated ALS/FTD (C9-ALS/FTD) (19–21).

Quality control of gene expression is central for sustaining cellular physiology and homeostasis. Nonsense-mediated decay (NMD), nonstop decay (NSD) and no-go decay (NGD) are three major pathways for mRNA surveillance that sense premature termination codons, stop-codon readthrough and translational stalling, respectively, during translation of mRNA (22–24). Subsequently, individual RNA control pathways recruit RNA-decaying factors to aberrant transcripts and promote their degradation. Translational stalling can occur when translating ribosomes encounter specific molecular signatures encoded in mRNAs. These include repetitive sequences of a specific codon or

*To whom correspondence should be addressed. Tel: +82 52 217 2554; Email: clim@unist.ac.kr
†The authors wish it to be known that, in their opinion, the first two authors should be regarded as Joint First Authors.

di-codon pairs, RNA damage or secondary structures that delay or are inhibitory to translational elongation (25). For instance, the translation of polyadenylated residues (poly-A) in coding regions of mRNA potently arrests translating ribosomes, thereby triggering the NGD pathway (23,26). Furthermore, ribosome-associated quality control (RQC) factors ensure the quality of translation products by co-translationally targeting aberrant nascent polypeptides for proteasomal degradation and facilitate the recycling of ribosomal subunits (27,28).

The RING-domain E3 ubiquitin ligase, zinc finger protein 598 (ZNF598), plays an essential role in initiating this process (29–37). Ribosomal collisions during translational stalling or in cells under stress cue ZNF598 and receptor for activated C kinase 1 (RACK1) to promote the ubiquitination of specific ribosomal proteins (i.e. RPS3, RPS10 and RPS20) in the 40S subunit (32–34,37,38), leading to RQC trigger complex-mediated dissociation of the 80S ribosomes stalled on RQC substrates (26,35). Nascent polypeptides entrapped in the 60S subunit are ubiquitinated for subsequent proteasomal degradation by the coordinated action of 60S-associating nuclear export mediator factor (NEMF) and listerin E3 ubiquitin-protein ligase 1 (LTN1) (28,39,40). The substrate-specificity of LTN1 in the quality control of premature translation products is conferred by its exclusive association with the 60S subunit in a complex with NEMF (41–45). In addition, NEMF mediates the C-terminal alanine/threonine (CAT)-tailing of RQC substrates (46–48). The mRNA template-independent process is thought to expose the internal lysine residues in the entrapped nascent chains to the LTN1 E3 ligase activity near the ribosome exit channel (45,49–51). The peptidyl-tRNA conjugate is further extracted from the 60S subunit by ANKZF1 and VCP (52–54), thereby facilitating ribosomal recycling.

Since poly-A translation possibly indicates errors in post-transcriptional gene expression (e.g. premature polyadenylation in the coding sequence and stop-codon readthrough), efficient removal of aberrant transcripts and nascent polypeptides by co-translational quality control pathways should play an essential role in supporting cellular proteostasis. Any impairment in quality control pathways, on the other hand, could cause a wide range of proteotoxic stress, leading to human diseases. Here, we show that coding sequences for ALS-relevant, pathogenic poly(GR) protein cause translational stalling and their ribosome-associated translation products are subject to degradation via the ZNF598-LTN1 pathway. We further demonstrate that C9-ALS patient-derived neurons display loss of RQC activity, whereas ZNF598 overexpression is sufficient to suppress their poly(GR) expression and apoptotic degeneration.

MATERIALS AND METHODS

Drosophila melanogaster

Flies were raised on standard cornmeal-yeast-agar medium (5.4% cornmeal, 1.3% yeast, 0.7% soy flour, 0.4% agar, 4.2% starch syrup, 0.4% propionic acid, 0.8% methyl 4-hydroxybenzoate) at 25°C. The fly lines, UAS-poly-GR.PO-36 (BL58692), UAS-poly-PR.PO-36 (BL58694), UAS-hATX1[82Q] (BL33818), UAS-hTDP43 (BL51371), UAS-Aβ42 (BL33769), UAS-*CG11414* RNAi (T61288, T67278), *Nulp1*[G6757] (BL27215), UAS-*Clbn* RNAi (T62402) and *Ltn1*[G9156] (BL30116) were obtained from Bloomington *Drosophila* Stock Center. Additional information for RNAi lines obtained from Bloomington *Drosophila* Stock Center, National Institute of Genetics, and Vienna *Drosophila* Resource Center can be found in Supplementary Table S1.

DNA constructs

GR_{100} cDNA (55) (a gift from D. Ito) was subcloned into a modified pcDNA3.1 for the expression of N-terminal GFP fusion proteins (GFP-GR_{100}). DNA clones harboring *C9ORF72*-derived hexanucleotide repeats ($GGGGCC_{60}$ or $GGGGCC_{115}$) (10) (gifts from L.P.W. Ranum) were modified to generate pcDNA3.1-based expression vectors for N-terminal GFP fusion proteins (GFP-c9GR_{60}, GFP-c9GR_{115}, GFP-c9GA_{115}). Expression vectors for FLAG-tagged ZNF598 (pcDNA3.1-ZNF598-TEV-3xFLAG, Addgene plasmid #105690) and FLAG-tagged $ZNF598^{\Delta RING}$ were gifts from R.S. Hegde (32). $ZNF598^{R69C}$ cDNA was generated by PCR-based mutagenesis from pcDNA3.1-ZNF598-TEV-3xFLAG and subcloned into the same vector backbone. Wild-type and mutant ZNF598 cDNAs were further PCR-amplified and subcloned into pcDNA3.1 to overexpress untagged ZNF598 proteins. Expression vectors for V5-tagged NEMF (pcDNA3.1-V5-NEMF, $NEMF^{D96A}$ and $NEMF^{DR96AA}$) and LTN1 (pCDH-EF1-LTN1 and LTN1 $^{\Delta RING}$) were gifts from T. Inada (48). S-tdT cDNA (14) (a gift from J.D. Rothstein) was subcloned into pcDNA3.1 to express the fluorescent reporter for nucleocytoplasmic transport. pmGFP-P2A-K0-P2A-RFP (Addgene plasmid #105686) and pmGFP-P2A-K(AAA)20-P2A-RFP (Addgene plasmid #105688) were gifts from R.S. Hegde (32). GR_{100}, PR_{100} and GA_{100} cDNAs (55) (gifts from D. Ito) were subcloned into pmGFP-P2A-K0-P2A-RFP to generate the P2A-based polycistronic fluorescent reporters, GR_{100}, PR_{100} and GA_{100}. DNA clones harboring $GGGGCC_{115}$ or $CCCCGG_{115}$ (10) (gifts from L.P.W. Ranum) were modified to generate the P2A-based translation reporters for *C9ORF72*-derived codon repeats, c9GR_{115}, c9PR_{115} and c9GA_{115}. These translation reporters were further subcloned into pcDNA3.1-based expression vectors for N-terminal GFP-fusion reporters (N-GFP-K0-P2A-RFP, N-GFP-K(AAA)20-P2A-RFP, N-GFP-GR_{100}-P2A-RFP, N-GFP-PR_{100}-P2A-RFP, N-GFP-GA_{100}-P2A-RFP). pRK5-HA-Ubiquitin-WT (Addgene plasmid #17608) and pRK5-HA-Ubiquitin-K0 (Addgene plasmid #17603) were gifts from T.M. Dawson (56). Recombinant lentiviral vectors for the pmGFP-P2A-K0-P2A-RFP and pmGFP-P2A-K(AAA)20-P2A-RFP reporters were constructed by the Gateway cloning of modified pENTR4 entry vectors (Addgene plasmid #17424) harboring the reporter cDNAs into pLenti-PGK-Puro-DEST destination vector (Addgene plasmid #19068). Recombinant lentiviral vectors for the overexpression of wild-type or mutant ZNF598 were constructed by the Gateway cloning of pENTR-*Ubiquitin C* promoter (Addgene plasmid #45959) and modified pENTR4-FLAG entry vectors (Addgene plasmid #17424)

harboring individual ZNF598 cDNAs into pCWX-DEST destination vector (Addgene plasmid #45957).

Cell culture

Human neuroblastoma SH-SY5Y cells and embryonic kidney 293T cells were cultured in Dulbecco's Modified Eagle Medium (HyClone) supplemented with 10% fetal bovine serum and 1% antibiotics. C9-ALS patient-derived induced pluripotent stem cell (iPSC) lines (CS28iALS, CS29iALS and CS52iALS) and control lines (CS0YX7iCTR, CS29iALS-ISO and CS4NWCiCTR) were obtained from the Cedars-Sinai iPSC Core. iPSCs were grown on mTeSR1 medium (STEMCELL Technologies) according to the standard Cedars-Sinai protocol and subsequently differentiated into neural progenitor cells (NPCs) and motor neurons (iPSNs) as described previously (18,57). Cell cultures were maintained at 37°C in a humidified incubator with 95% air and 5% CO_2. SH-SY5Y cells were transiently transfected with plasmid DNA and siRNA using polyethyleneimine (58) and Lipofectamine RNAiMAX transfection reagent (Thermo Fisher Scientific), respectively, according to the manufacturer's instructions. The siRNA sequences for ZNF598 depletion (5′-GAA AGG UGU ACG CAU UGU A-3′), LTN1 depletion (5′-GAG AGU ACC UUC CUA CAU U-3′) and non-targeting control (5′-CCU CGU GCC GUU CCA UCA GGU AGU U -3′) have been described previously (18,33,59). 293T cells were co-transfected with viral packaging plasmids (ViraPower Lentiviral Packaging Mix; Invitrogen) and recombinant lentiviral destination vectors. Cell culture medium containing recombinant lentiviruses was harvested 48 and 72 h after transfection. Lentiviral particles were then concentrated by ultracentrifugation at 25 000 rpm for 4 h at 4°C. NPCs were transduced with concentrated aliquots of recombinant lentiviruses in the presence of 1 μg/ml polybrene for 12 h to overexpress translation reporters or 5 μg/ml polybrene for 6 h to overexpress wild-type or mutant ZNF598 protein. iPSNs were harvested 7–9 days or 21 days after motor neuron differentiation from NPCs and subsequently analyzed.

Establishment of *ZNF598*^{KO}, *NEMF*^{KO} and *LTN1*^{KO} cell lines

Small guide RNA (sgRNA) sequence for CRISPR/Cas9-mediated *NEMF* deletion (5′-TCA GCT CCG CGA GTA CGG CG-3′) was designed using CHOPCHOP (https://chopchop.rc.fas.harvard.edu). The sgRNA sequences for *ZNF598* deletion (5′-TAG AGC AGC GGT AGC ACA CC-3′) and *LTN1* deletion (5′-ATT CCA CCA CAA CCT AAC CA-3′) have been described previously (32,60). The oligonucleotides encoding individual sgRNAs were synthesized (Macrogen) and subcloned into pRGEN-U6-sgRNA and pHRS (ToolGen) for the expression of gene-specific sgRNA and hygromycin B-resistance reporter gene, respectively. SH-SY5Y cells were co-transfected with pRGEN-Cas9-CMV, pRGEN-U6-sgRNA and pHRS-sgRNA reporters. Reporter-edited cells were selected by culturing in medium containing hygromycin B (500 μg/ml) for 2 weeks. Independent cell lines were established by seeding individual colonies into 6-well cell plates containing hygromycin B-free media. Total cell extracts were prepared from individual cell lines and analyzed by immunoblotting with gene-specific antibodies to monitor target gene expression.

Immunofluorescence assay

Cells grown on coverslips were fixed in phosphate-buffered saline (PBS) containing 3.7% formaldehyde at room temperature for 15 min. Fixed cells were washed twice with PBS and permeabilized with PBS containing 0.1% Triton X-100 (PBS-T) at 4°C for 15 min. After two washes with PBS, permeabilized cells were blocked with PBS-T containing 1% bovine serum albumin at room temperature for 30 min and then incubated with blocking buffer containing primary antibodies and 0.05% sodium azide at 4°C overnight. The primary antibodies used in immunostaining were mouse anti-FLAG (1:1,000 dilution; Sigma-Aldrich), rabbit anti-lamin B1 (1:1000 dilution; Proteintech), rabbit anti-G3BP1 (1:1000 dilution; Proteintech), rabbit anti-poly(GR) (1:250; Proteintech), rabbit anti-poly(PR) (1:250; Proteintech), rabbit anti-cleaved caspase-3 (1:400; Cell Signaling Technology) and guinea pig anti-MAP2 (1:1000; Synaptic System). Cells were washed twice with PBS-T for 5 min each and then incubated with PBS-T containing secondary antibodies at 4°C overnight. Species-specific Alexa Flour 594- or 647-conjugated anti-IgG antibodies were used as secondary antibodies for immunostaining (1:600 dilution; Jackson ImmunoResearch Laboratories). Nuclei were visualized by staining with Hoechst 33258 for 5 min. Stained samples were washed twice with PBS-T and then mounted on imaging slides using VECTASHIELD antifade mounting medium (Vector Laboratories).

Quantitative image analysis

Confocal images were obtained using an FV1000 microscope (Olympus). Random fields of interest in each imaging sample were scanned using identical imaging settings. Fluorescence intensities in individual cells were quantified using ImageJ software. For analyses of nuclear lamina integrity and DPR granule formation, the percentage of cells with abnormal patterns of anti-lamin B1 staining per confocal image, the number of nuclear poly(GR) granules per cell, the number of cytoplasmic poly(GR) granules per cell, the number of G3BP1–positive stress granules per cell and the number of cytoplasmic poly(GA) granules per cell were manually scored. The relative distribution of S-tdT between nucleus and cytoplasm (N/C ratio) was quantified by calculating the ratio of nuclear to cytoplasmic fluorescence from the reporter protein per cell. For analyses of poly(GR) and poly(PR) granules in C9-ALS iPSNs, confocal images of several random fields were *z*-stacked with maximum intensity projection. The defined region of interest (ROI) was then traced within a MAP2–positive neurite. Fluorescence intensities above a threshold were unbiasedly quantified by ImageJ Analyze Particles plugin to count granule numbers and measure their size. The number of granules was then normalized to the length of each neurite using the ImageJ Measure plugin.

Flow cytometry analysis

Transfected cells were trypsinized 48 h after transfection, collected by centrifugation at 2000 rpm for 3 min at room temperature and then resuspended in PBS. GFP and mCherry reporter protein fluorescence per cell was quantified using LSRFortessa (BD Biosciences) and analyzed in 20 000 GFP–positive cells using FlowJo software.

Immunoblotting

Dot-blot analyses of *Drosophila* head extracts were performed as described previously (61) with minor modifications. Briefly, adult fly heads were homogenized in RIPA buffer (50 mM Tris-Cl pH 8.0, 150 mM NaCl, 5 mM EDTA, 1% NP-40 (v/v), 0.5% sodium deoxycholate, 0.1% sodium dodecyl sulfate [SDS]) containing 1 mM phenylmethylsulfonyl fluoride (PMSF) and 1 mM dithiothreitol (DTT) and diluted in 1× SDS sample buffer. After boiling for 5 min, 1.25 μl of serially diluted samples were dot-blotted on Protran nitrocellulose membranes (GE Healthcare) to detect actin protein. Head extracts were further digested with 10 μg/ml of proteinase K at 37°C for 1 h, boiled for 5 min and dot-blotted on the nitrocellulose membranes to detect poly(GR) and poly(PR) proteins. Membranes were dried for 15 min and incubated with a specific set of antibodies. Protein samples from human cell cultures were resolved by SDS-PAGE, transferred to the nitrocellulose membranes and incubated with a specific set of primary antibodies. The primary antibodies used in immunoblotting were rabbit anti-actin (1:1000; Sigma), rabbit anti-poly(GR) (1:1000; Proteintech), rabbit anti-poly(PR) (1:1000; Proteintech), rabbit anti-GFP (1:1000; Santa Cruz Biotechnology), mouse anti-GFP (1:1000; Santa Cruz Biotechnology), rabbit anti-mCherry (1:1000; BioVision), mouse anti-Dsred (1:1000; Santa Cruz Biotechnology), mouse anti-FLAG (1:1000; Sigma), rabbit anti-FLAG (1:1000; Sigma), rabbit anti-ZNF598 (1:1000; Bethyl Laboratories), rabbit anti-NEMF (1:1000; Bethyl Laboratories), rabbit anti-LTN1 (1:1000; Invitrogen), mouse anti-RACK1 (1:2000; Santa Cruz Biotechnology), rabbit anti-EDF1 (1:2000; Bethyl Laboratories), mouse anti-RPS6 (1:1000; Santa Cruz Biotechnology), rabbit anti-RPS10 (1:1000; Abcam), rabbit anti-RPS20 (1:1000; Novus biologicals), mouse anti-RPLP0 (1:1000; Santa Cruz Biotechnology), rabbit anti-tubulin (1:1000; Proteintech) and mouse anti-tubulin antibodies (1:1000; Developmental Studies Hybridoma Bank). Immunoreactive proteins were recognized by species-specific horseradish peroxidase-conjugated secondary antibodies (Jackson ImmunoResearch Laboratories) and subsequently detected with Clarity Western ECL blotting substrate (Bio-Rad) using ImageQuant LAS 4000 (GE Healthcare) and iBright1500 (Thermo Fisher).

Sucrose cushion fractionation

Transfected cells on a 100-mm dish were incubated with cycloheximide (CHX; 100 μg/ml) for 10 min before harvesting. Cell pellets were lysed at 4°C in sucrose cushion buffer (50 mM Tris-Cl pH 7.5, 5 mM $MgCl_2$, 25 mM KCl) containing 0.5% NP-40 (v/v), 1 mM PMSF and 1 mM DTT. Where indicated, 100 μg/ml of RNase A was added to the cushion buffer. Small aliquots of the cell lysates served as input in immunoblotting. The remainder of the cell lysates was loaded on a 35% (w/v) sucrose cushion in the cushion buffer and centrifuged at 38 000 rpm for 3 h in an SW41Ti rotor (Beckman Coulter). After centrifugation, the pellet was resuspended in the lysis buffer while the supernatant was further concentrated by methanol/chloroform precipitation. Protein samples from input, pellet and supernatant fractions were resolved by SDS-PAGE and then analyzed by immunoblotting (see above).

Sucrose density gradient fractionation

Transfected cells on a 100-mm dish were incubated with 100 μg/ml of CHX for 10 min before harvesting. Cell pellets were lysed in sucrose density gradient buffer (50 mM Tris-Cl pH 7.5, 10 mM $MgCl_2$, 25 mM KCl, 0.1 mg/ml heparin, 50 U/ml RNase inhibitor) containing 0.5% NP-40 (v/v), 1 mM PMSF and 1 mM DTT at 4°C for 15 min with gentle rocking. After clarification by centrifugation, soluble extracts were loaded on top of 10–50% (w/v) or 10–40% (w/v) sucrose density gradient solution and centrifuged at 38 000 rpm for 2 or 5 h, respectively, in an SW41Ti rotor (Beckman Coulter). Using Minipuls 3 (Gilson) and tube piercer (Brandel), gradient samples were fraction-collected into 1.5 ml tubes while UV absorbance at 254 nm was monitored continuously with a UA-6 detector (ISCO). Protein samples were prepared from individual fractions by methanol/chloroform precipitation, resolved by SDS-PAGE and then analyzed by immunoblotting (see above).

Immunoprecipitation

Transfected cells on a 100-mm dish were incubated with 100 μg/ml of CHX for 10 min before harvesting. Cell pellets were lysed in lysis buffer (25 mM Tris-Cl pH 7.5, 150 mM NaCl, 10% glycerol, 5 mM $MgCl_2$, 0.5% NP-40 (v/v), 1 mM PMSF, 1 mM DTT, 100 μg/ml CHX) at 4°C for 15 min with gentle rocking. After clarification by centrifugation, soluble extracts were incubated with anti-FLAG M2 affinity gel (Sigma) at 4°C for 1.5 h with gentle rocking. The beads were then washed five times in the same buffer. For detecting the polyubiquitination of translation reporter proteins, cell lysis and immunoprecipitation were performed using the RIPA buffer containing 1 mM PMSF, 1 mM DTT and 100 μg/ml CHX. Immunoprecipitated samples were eluted by boiling in SDS sample buffer for 5 min, resolved by SDS-PAGE and then analyzed by immunoblotting (see above).

Quantitative transcript analysis

Total RNA was purified using RNeasy Mini kit (Qiagen) according to the manufacturer's instruction. RNA samples were reverse-transcribed using M-MLV transcriptase (Promega) with random hexamers. Diluted cDNA samples were quantitatively analyzed using Prime Q-Mastermix (GeNetBio) and pairs of gene-specific primers on LightCycler 480 real-time PCR system (Roche). Additional information for primer sequences can be found in Supplementary Table S2.

Statistical analysis

Microsoft Excel and GraphPad Prism were used for Student's *t*-test, one-way analysis of variance (ANOVA), two-way ANOVA with post hoc tests and frequency distribution analysis. The statistical details of experiments, including the number of samples analyzed, the statistical tests used and *P* values were described in the figure legends.

RESULTS

A *Drosophila* screen identifies a *ZNF598*-relevant RQC pathway as a genetic modifier of *C9ORF72*-derived poly(GR) toxicity

To elucidate molecular pathways that contribute to the neurotoxicity of *C9ORF72*-derived DPR proteins, we performed a genetic modifier screen in *Drosophila* (Figure 1A). Transgenic overexpression of poly(GR) or poly(PR) protein induces degeneration in the *Drosophila* photoreceptor neurons, disrupting their organization of ommatidia (61). Co-expression of individual RNA interference (RNAi) transgenes targeting 129 RNA-binding proteins or factors relevant to RNA granules (i.e. stress granule or processing-body) led us to the identification of 51 genetic modifiers for the poly(GR) or poly(PR) toxicity (Figure 1B and Supplementary Table S1). Several of these modifier genes were consistently identified in previous studies (62–65), justifying our genetic approach. Intriguingly, we found that transgenic depletion of *CG11414* (a *Drosophila* homolog of *ZNF598*) in poly(GR)-expressing photoreceptor neurons severely deformed the compound eye while negligibly affecting control neurons (Figure 1C). Degenerative effects on poly(GR)-expressing neurons were similarly observed using two independent $ZNF598^{RNAi}$ transgenes, likely excluding off-target effects. Dot-blot analyses of extracts from whole fly heads revealed that poly(GR) protein was not detectable in ZNF598-depleted neurons, possibly owing to their severe degeneration during development (Supplementary Figure S1). ZNF598 effects on poly(PR) toxicity were relatively weak, and ZNF598 depletion did not significantly affect poly(PR) levels in the photoreceptor neurons. Nonetheless, transgenic depletion of additional RQC factors similarly caused degeneration or necrotic patches in DPR-overexpressing neurons, but not in control neurons (Figure 1C). We further found that these RQC factors did not comparably modify the neurotoxicity of other pathogenic proteins involved in neurodegenerative diseases (e.g. hATX1[82Q], hTDP43, Aβ42) (Figure 1D). These pieces of genetic evidence indicate that ZNF598 and other RQC factors specifically suppress poly(GR) toxicity in a *Drosophila* model of C9-ALS/FTD.

ZNF598 overexpression suppresses the cytotoxic effects of poly(GR) protein

To determine if *ZNF598* effects on poly(GR) toxicity are evolutionarily conserved, we generated human neuroblastoma cells that either harbored a genomic deletion in the *ZNF598* locus (hereafter, $ZNF598^{KO}$) or transiently overexpressed ZNF598 proteins. We employed a poly(GR) transgene that encoded a green fluorescent protein-fused poly(GR) protein ($GFP\text{-}GR_{100}$) in a codon sequence redundant to the *C9ORF72*-associated hexanucleotide repeats (GGGGCC). Cytotoxic effects of the transgenic poly(GR) protein were then examined in different genetic backgrounds. Overexpression of $GFP\text{-}GR_{100}$ disrupted the integrity of the nuclear lamina (Figure 2A), as shown by anti-lamin B1 staining, and interfered with nucleocytoplasmic transport of the reporter protein, shuttle-tdTomato (Figure 2B) to a comparable degree in control and $ZNF598^{KO}$ cells. Intriguingly, however, we found that overexpression of wild-type ZNF598 protein efficiently abrogated $GFP\text{-}GR_{100}$ effects on both nuclear phenotypes regardless of *ZNF598* deletion. ZNF598 has a conserved RING domain that is crucial for the E3 ubiquitin ligase activity and RQC function (32–34). We searched for mutant *ZNF598* alleles in the Project MinE database (http://databrowser.projectmine.com/) established by a large-scale whole-genome sequencing study in ALS (66) and identified a missense mutant allele of the RING domain ($ZNF598^{R69C}$) in ALS patient. $ZNF598^{R69C}$ allele was not reported in other general databases for single-nucleotide polymorphism, such as the Genome Aggregation Database (https://gnomad.broadinstitute.org/) or the Single Nucleotide Polymorphism Database (https://www.ncbi.nlm.nih.gov/snp/). In contrast to wild-type ZNF598, overexpression of RING domain-deleted mutant ($ZNF598^{\Delta RING}$) or ALS-relevant mutant ($ZNF598^{R69C}$) did not significantly affect poly(GR) toxicity in either control or $ZNF598^{KO}$ cells (Figure 2A and B), suggesting their loss-of-function properties.

We further found that nuclear accumulation of $GFP\text{-}GR_{100}$ protein, indicated by GFP–positive nuclear granules, was facilitated in $ZNF598^{KO}$ cells, whereas overexpression of wild-type ZNF598 blocked it (Figure 2C). Overexpression of wild-type ZNF598, but not mutant ZNF598 (i.e. $ZNF598^{\Delta RING}$ or $ZNF598^{R69C}$), similarly suppressed the nuclear accumulation of $GFP\text{-}c9GR_{60}$ protein encoded by the *C9ORF72*-associated GGCCGG repeats, likely indicating a codon-independent regulation. These observations may explain why ZNF598 overexpression suppresses the two nuclear phenotypes in poly(GR)-expressing cells (Figure 2A and B). We also reasoned that the cytotoxic effects of the nuclear GR granules might be saturated already in control cells, and thus we failed to detect severer phenotypes in $ZNF598^{KO}$ cells. Smaller numbers of cytoplasmic GR granules and G3BP1–positive stress granules (14) were detected in poly(GR)-overexpressing cells under the same conditions (Figure 2C), but we observed no significant effects of *ZNF598* on those two cytoplasmic granules (Supplementary Figure S2A). Also, the cytoplasmic accumulation of poly(GA) protein encoded by the alternative reading frame of *C9ORF72* repeats (i.e. GGGGCC) was insensitive to the *ZNF598* gene dosage (Supplementary Figure S2B), further validating specific effects of *ZNF598* on the nuclear GR granules. Immunoblotting analyses revealed that $ZNF598^{KO}$ cells expressed high levels of $GFP\text{-}GR_{100}$ protein and overexpression of wild-type ZNF598, but not mutant ZNF598, rescued the loss-of-function effects (Supplementary Figure S3). However, $GFP\text{-}GR_{100}$ levels in control cells were not significantly affected by ZNF598 overexpression, contrasting with its strong suppression of the nuclear GR assembly. These results suggest that ZNF598

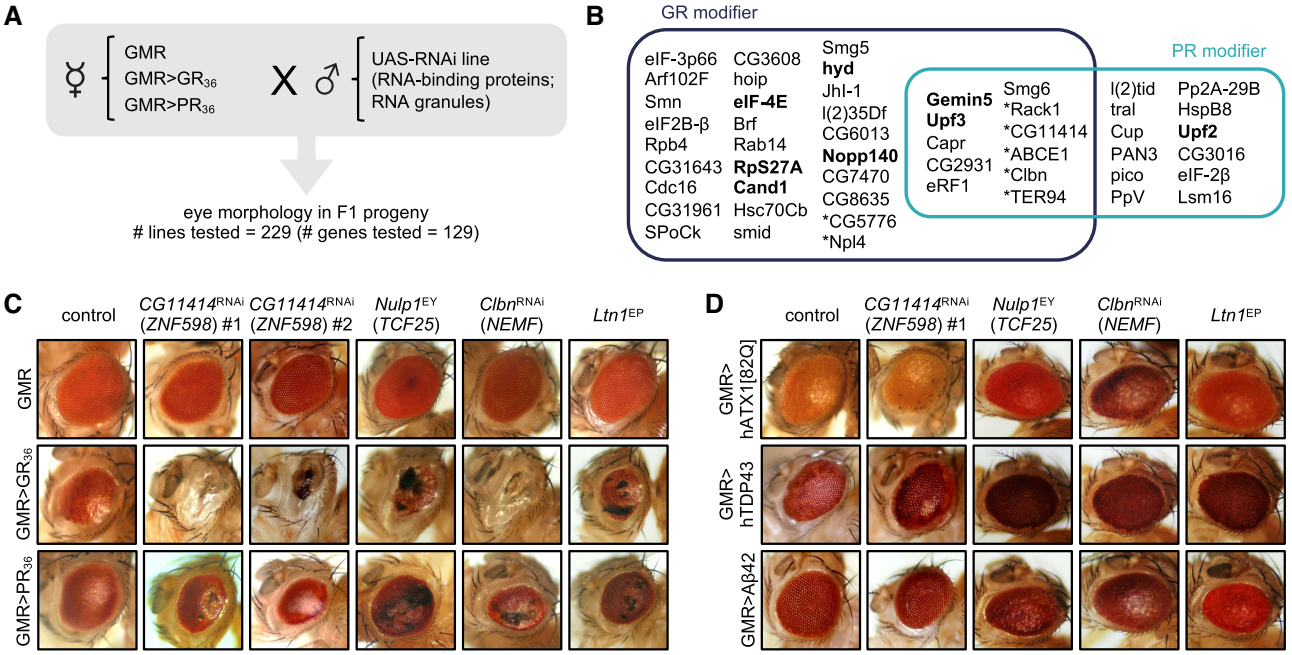

Figure 1. Loss of RQC function exacerbates the neurodegenerative effects of *C9ORF72*-derived DPR proteins in *Drosophila*. (**A**) A scheme of the *Drosophila* genetic screen for modifiers of *C9ORF72*-derived DPR toxicity. Virgin flies overexpressing poly(GR) or poly(PR) protein in the photoreceptor neurons (GMR > GR_{36} or GMR > PR_{36}) were crossed to individual RNAi lines targeting RNA-binding proteins or factors relevant to RNA granules (stress granules and processing-bodies/P-bodies). Additive or non-additive eye phenotypes were scored in F1 progeny. (**B**) A list of modifier genes of which depletion exaggerates the eye degeneration by poly(GR), poly(PR) or both proteins. Asterisks, *Drosophila* homologs implicated in the RQC pathway; gene names in bold, published genetic modifiers of *C9ORF72*-derived DPR toxicity. (**C**) Transgenic overexpression of GR_{36} or PR_{36} protein in the *Drosophila* photoreceptor neurons disrupted the organization of ommatidia. Transgenic RNAi depleted a *Drosophila* homolog of *ZNF598* (*CG11414*) or *NEMF* (*Clbn*) in DPR-expressing photoreceptor neurons. Alternatively, the heterozygous mutation in a *Drosophila* homolog of *TCF25* ($Nulp1^{EY}$) or *LTN1* ($Ltn1^{EP}$) was genetically introduced to DPR-expressing photoreceptor neurons. Black patches indicate necrotic cells. (**D**) Transgenic depletion of individual RQC factors negligibly affected the degenerative effects of other pathogenic proteins involved in neurodegenerative diseases.

may limit both quantity and quality of poly(GR) expression, thereby reducing their nuclear accumulation and cytotoxicity. This activity requires the ZNF598 RING domain and is impaired by the ALS-relevant *ZNF598* mutation.

The ALS-relevant *ZNF598* allele causes loss-of-function effects on the canonical RQC substrate

The E3 ubiquitin ligase ZNF598 senses ribosomal stalling during poly-A translation and promotes the ubiquitination of specific ribosomal proteins (e.g. RPS3, RPS10, RPS20) (32–34,37–38). This activity triggers the RQC pathway, leading to ribosomal disassembly from the translating RNA substrate by the RQC trigger complex and subsequent ribosome recycling (35,67). Lack of $ZNF598^{R69C}$ effects on the nuclear accumulation and toxicity of poly(GR) prompted us to ask if the ALS-relevant *ZNF598* mutation would cause loss-of-function effects on the canonical RQC substrate. To test this, we employed a polycistronic RNA reporter containing 20 repeats of the lysine-encoding AAA codon (hereafter, $K(AAA)_{20}$ reporter) (Figure 3A) and assessed ZNF598-dependent RQC activity (32–34).

We first validated that *ZNF598* deletion rescued the translational stalling of the $K(AAA)_{20}$ reporter, as assessed by a high ratio of mCherry to GFP expression in $ZNF598^{KO}$ cells (Figure 3B). On the other hand, ZNF598 overexpression enhanced RQC activity in both wild-type and $ZNF598^{KO}$ cells (Figure 3C), consistent with previous observations (32–34). Under similar conditions, overexpression of either $ZNF598^{\Delta RING}$ or $ZNF598^{R69C}$ negligibly affected the translation stalling of the $K(AAA)_{20}$ reporter (Figure 3C). Immunoblotting analyses of the reporter expression confirmed that ZNF598 overexpression selectively suppressed the translation of $K(AAA)_{20}$ (i.e. FLAG-K_{20}) and its downstream reporter gene (i.e. mCherry) (Figure 3D and E). Furthermore, ZNF598 overexpression generated translationally arrested products (APs) on the $K(AAA)_{20}$ repeat (32). By contrast, overexpression of $ZNF598^{\Delta RING}$ or $ZNF598^{R69C}$ in $ZNF598^{KO}$ cells failed to suppress the expression of FLAG-K_{20} and mCherry to the same extent as wild-type ZNF598 (Figure 3C–E). We further found that these ZNF598 mutants did not support ZNF598-dependent ubiquitination of ribosomal proteins (Figure 3F).

Translational stalling occurs on coding sequences for arginine-containing DPR proteins

The strong correlation of RQC activity with the suppression of poly(GR) toxicity among *ZNF598* alleles suggests the simple hypothesis that translation of poly(GR)-encoding mRNA may cause ribosomal stalling. The ZNF598-dependent RQC pathway would then dissociate the stalled ribosomes from the poly(GR)-encoding mRNA, suppressing poly(GR) translation. To test this hypothesis, we generated a series of polycistronic reporters that expressed DPR proteins from the original hexanucleotide repeats in the

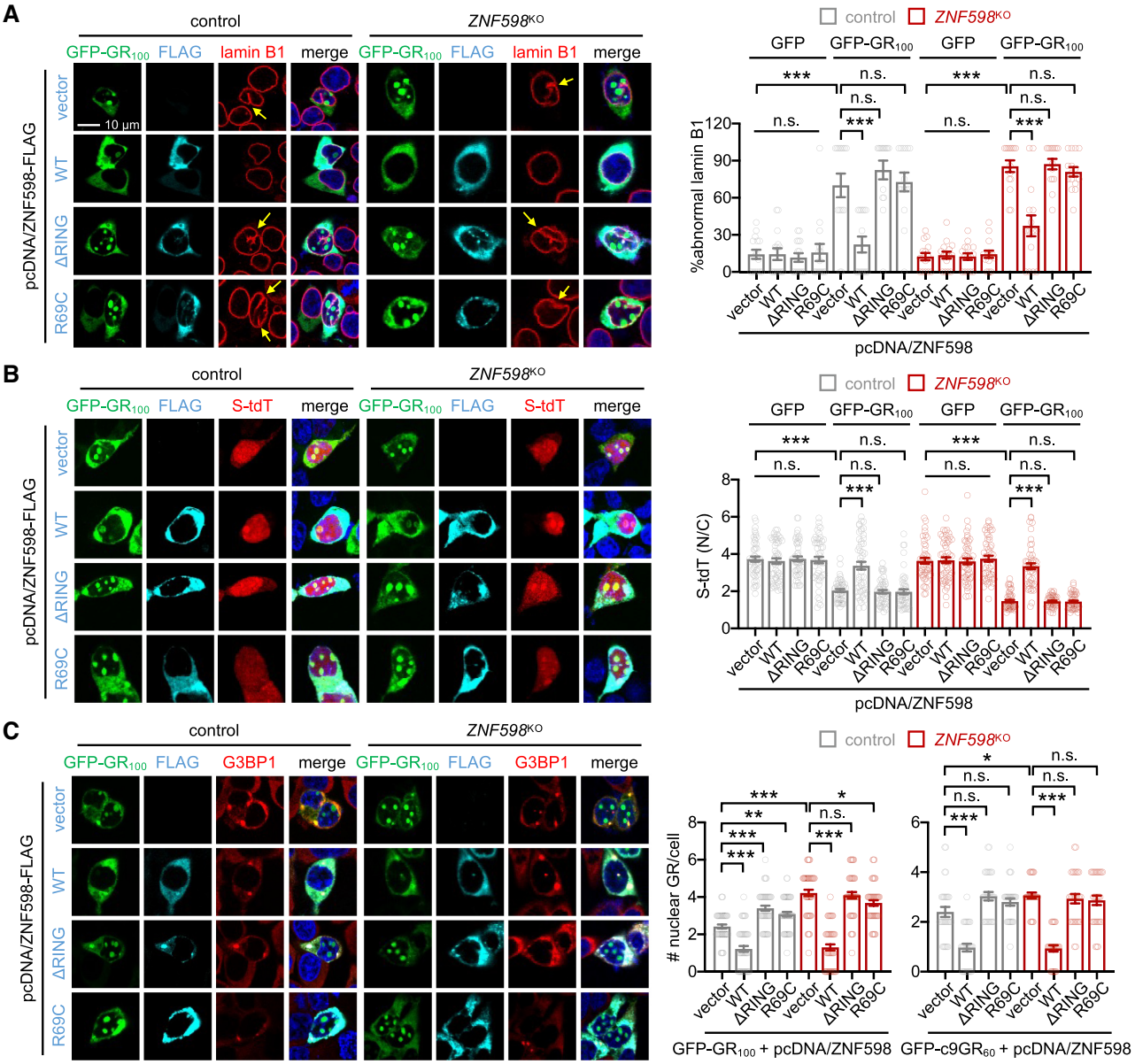

Figure 2. ZNF598 reduces poly(GR) cytotoxicity in human neuroblastoma cells. (**A**) ZNF598 overexpression suppresses poly(GR)-induced disruption of the nuclear lamina. Control and *ZNF598*-deleted SH-SY5Y cells ($ZNF598^{KO}$) were co-transfected with expression vectors for GFP-GR_{100} and FLAG-tagged ZNF598 proteins (wild-type, $ZNF598^{\Delta RING}$, or $ZNF598^{R69C}$). Transfected cells were co-stained with anti-FLAG antibody (cyan), anti-lamin B1 antibody (red), and Hoechst 33258 (blue) 36 h after transfection. Yellow arrows indicate GFP-GR_{100}–positive cells with disruption of the nuclear lamina. Data represent means ± SEM ($n = 15$ confocal images; $n = 33$–148 GFP– or GFP-GR_{100}–positive cells). n.s., not significant; $^{***}P < 0.001$, as determined by two-way ANOVA with Tukey's multiple comparisons test. (**B**) ZNF598 overexpression suppresses poly(GR)-induced disruption of nucleocytoplasmic transport. Control and $ZNF598^{KO}$ cells were co-transfected with expression vectors for GFP-GR_{100}, shuttle-tdTomato (S-tdT), and FLAG-tagged ZNF598 proteins. Transfected cells were co-stained with anti-FLAG antibody (cyan) and Hoechst 33258 (blue) 36 hours after transfection. Nucleocytoplasmic transport of S-tdT reporter protein was quantified by calculating the ratio of nuclear to cytoplasmic (N/C) fluorescence in individual cells. Data represent means ± SEM (n = 50 GFP– or GFP-GR_{100}–positive cells). n.s., not significant; $^{***}P < 0.001$, as determined by two-way ANOVA with Tukey's multiple comparisons test. (**C**) ZNF598 overexpression suppresses nuclear accumulation of poly(GR) granules, whereas *ZNF598* deletion facilitates it. Control and $ZNF598^{KO}$ cells were co-transfected with expression vectors for GFP-GR_{100}/GFP-c9GR_{60} and FLAG-tagged ZNF598 proteins. Transfected cells were co-stained with anti-FLAG antibody (cyan), anti-G3BP1 antibody (red) and Hoechst 33258 (blue) 36 h after transfection to visualize FLAG-tagged ZNF598 proteins, stress granules and nuclei, respectively. The number of nuclear poly(GR) granules per cell was quantified and averaged from 50 GFP-GR_{100}–positive cells or 30 GFP-c9GR_{60}–positive cells. Error bars indicate SEM. n.s., not significant; $^{*}P < 0.05$, $^{**}P < 0.01$, $^{***}P < 0.001$, as determined by two-way ANOVA with Tukey's multiple comparisons test.

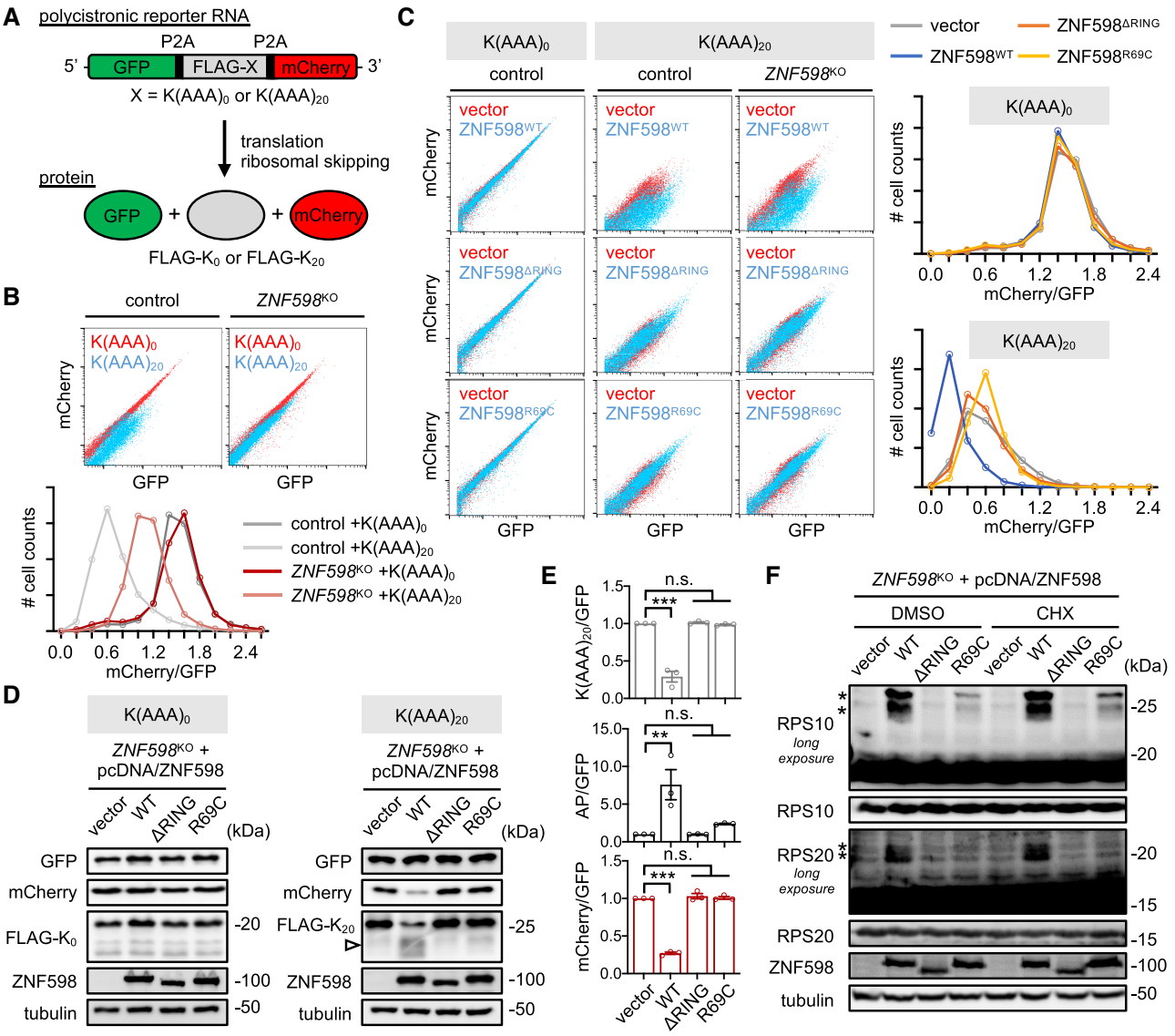

Figure 3. The ALS-relevant *ZNF598* allele causes loss-of-function effects on the canonical RQC substrate. (**A**) Schematic depiction of P2A-based polycistronic reporters encoding GFP and mCherry separated by FLAG-tagged $K(AAA)_0$ or $K(AAA)_{20}$ protein. (**B**) *ZNF598* deletion rescues translational stalling on the $K(AAA)_{20}$ reporter. Control and $ZNF598^{KO}$ cells were transfected with an expression vector for the $K(AAA)_0$ or $K(AAA)_{20}$ translation reporter. Fluorescent reporter expression was assessed in 20 000 cells using flow cytometry 48 h after transfection. Histograms for the ratio of mCherry to GFP expression were analyzed as a quantitative proxy for the relative distribution of fluorescent reporter-expressing cells in flow cytometry analyses. (**C**–**E**) Overexpression of wild-type ZNF598, but not mutant ZNF598 ($ZNF598^{\Delta RING}$ or $ZNF598^{R69C}$), enhances translational stalling on the $K(AAA)_{20}$ reporter and generates translationally arrested products (APs). Control and $ZNF598^{KO}$ cells were co-transfected with expression vectors for each translation reporter and transgenic ZNF598 proteins. Fluorescent reporter expression was analyzed by flow cytometry (C) or immunoblotting (D and E). Total extracts from transfected cells were resolved by SDS-PAGE and immunoblotted with the indicated antibodies. The band intensities for individual reporter proteins were measured and normalized to that for GFP in each genetic background. The relative levels of FLAG-tagged $K(AAA)_{20}$, APs (white arrowhead), and mCherry were then calculated by normalizing to vector control (set as 1). Data represent means ± SEM ($n = 3$). n.s., not significant; $^{**}P < 0.01$, $^{***}P < 0.001$, as determined by one-way ANOVA with Dunnett's multiple comparisons test. (**F**) Overexpression of wild-type ZNF598, but not mutant ZNF598, promotes ubiquitination of the ribosomal proteins RPS10 and RPS20. $ZNF598^{KO}$ cells were transfected with an expression vector for wild-type or mutant ZNF598 protein. Where indicated, transfected cells were incubated with cycloheximide (CHX; 100 μg/ml) or DMSO (vehicle control) 2 h before harvesting to inhibit translation elongation and induce ribosomal stalling. Total cell extracts were resolved by SDS-PAGE and immunoblotted with the indicated antibodies. Asterisks indicate ubiquitinated ribosomal proteins, as assessed by mobility shifts in SDS-PAGE.

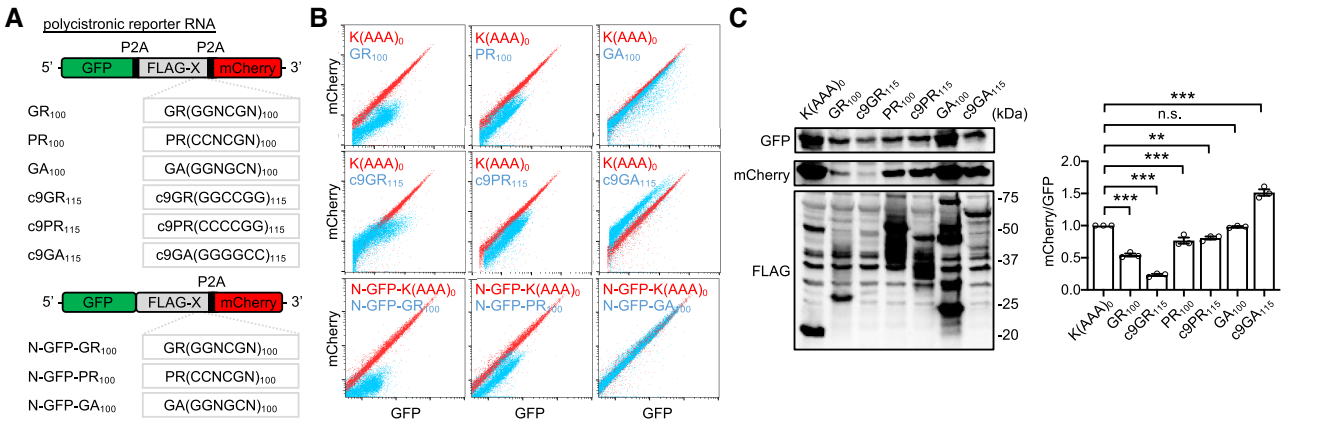

Figure 4. Translational stalling occurs on coding sequences for arginine-containing DPR proteins. (**A**) Schematic depiction of P2A-based polycistronic reporters encoding GFP and mCherry proteins separated by FLAG-tagged DPR proteins. GR, PR and GA reporters include 100 copies of hexanucleotides with degenerate bases, whereas c9GR, c9PR and c9GA reporters harbor 115 copies of the original *C9ORF72* hexanucleotide in different reading frames. (**B** and **C**) SH-SY5Y cells were transfected with an expression vector for each translation reporter. Fluorescent reporter expression was analyzed using flow cytometry (B) or immunoblotting (C), as in Figure 3. The band intensity for mCherry protein was measured and normalized to that for GFP in each genetic background. The relative levels of mCherry/GFP expression were then calculated by normalizing to the $K(AAA)_0$ control reporter (set as 1). Data represent means ± SEM ($n = 3$). n.s., not significant; $^{**}P < 0.01$, $^{***}P < 0.001$, as determined by one-way ANOVA with Dunnett's multiple comparisons test.

C9ORF72 locus (i.e. $c9GR_{115}$, $c9PR_{115}$, $c9GA_{115}$) or their redundant codons (i.e. GR_{100}, PR_{100}, GA_{100}) (Figure 4A) and examined effects of individual repeats on reporter expression. Flow cytometry analyses revealed that GR_{100} and PR_{100} repeats suppressed the relative expression of mCherry downstream of the repetitive sequences (Figure 4B and Supplementary Figure S4), consistent with a previous observation (68). $c9GR_{115}$ and $c9PR_{115}$ repeats displayed similar effects on the mCherry expression. On the other hand, GA_{100} repeat did not comparably affect the reporter expression, whereas $c9GA_{115}$ repeat increased rather than decreased the ratio of mCherry to GFP expression, possibly owing to RAN translation of the mCherry reporter (8,10). Immunoblotting analyses further confirmed the low ratio of mCherry to GFP expression from poly(GR) and poly(PR) reporters, although there were some variations in GFP expression from individual reporters (Figure 4C). It was unlikely that any ribosomal frameshifting on these repetitive coding-sequences would have abolished the downstream mCherry expression since no remarkable out-of-frame expression was detected in the DPR-encoding reporters (Supplementary Figure S4). These results support that the translation products of alternating arginine residues, but not of a specific arginine codon, may cause the arrest of translating ribosomes and thereby decrease the efficiency of downstream reporter translation. These observations contrast with the codon-specific activity of the canonical RQC pathway, which acts on K(AAA) repeats but not on K(AAG) repeats in mammalian cells (32–34).

ZNF598 down-regulates poly(GR) expression in a manner distinct from canonical RQC activity

If translational stalling on poly(GR)- or poly(PR)-encoding sequences is subject to canonical RQC, the ratio of mCherry to GFP expression from these arginine-containing reporters should be governed by the *ZNF598* gene dosage. However, we could not observe any consistent effects of *ZNF598* on their flow cytometry profiles (Supplementary Figure S5). One possible explanation would be that these repetitive sequences induced downstream mCherry expression by RAN translation. We indeed found that poly(GR) reporters expressed mCherry at detectable levels in flow cytometry analyses when stop codons were inserted in all reading frames between GFP- and poly(GR)-encoding sequences (Supplementary Figure S6). Moreover, their mCherry expression was not sensitive to the *ZNF598* gene dosage (Supplementary Figure S7). Another concern was that the P2A-mediated ribosomal skipping might cause short nascent chains of the arginine repeats to slip out of the dissociated 60S ribosomal subunit, bypassing the canonical RQC via LTN1-dependent proteasomal degradation. We thus generated additional GFP-fusion reporters (hereafter, N-GFP reporters) (Figure 4A) and examined RQC effects on their expression.

Immunoblotting of the translation products from the N-GFP-GR_{100} reporter revealed slow- and fast-migrating bands for poly(GR) protein in SDS-PAGE (Figure 5A). Biochemical fractionation using a sucrose cushion indicated that the slow-migrating proteins were associated with ribosome, whereas the fast-migrating band corresponded to ribosome-free poly(GR) protein (Supplementary Figure S8). Both poly(GR) products showed high expression levels in genomic deletion cell lines for *ZNF598* and *NEMF* (Figure 5A). An RNA-dependent mechanism may not explain RQC effects on the poly(GR) expression since the relative levels of N-GFP-$K(AAA)_{20}$ reporter RNA, but not of the other N-GFP reporter RNAs, were elevated in $ZNF598^{KO}$ cells (Supplementary Figure S9). Overexpression of wild-type ZNF598, but not of RQC-defective ZNF598 mutants (i.e. $ZNF598^{\Delta RING}$ and $ZNF598^{R69C}$), reduced the levels of both slow- and fast-migrating poly(GR) proteins in $ZNF598^{KO}$ cells (Figure 5B). Pharmacological inhibition of proteasome activity suppressed the ZNF598-overexpression effects (Figure 5C), suggesting that ZNF598 overexpression may facilitate the proteasomal degradation

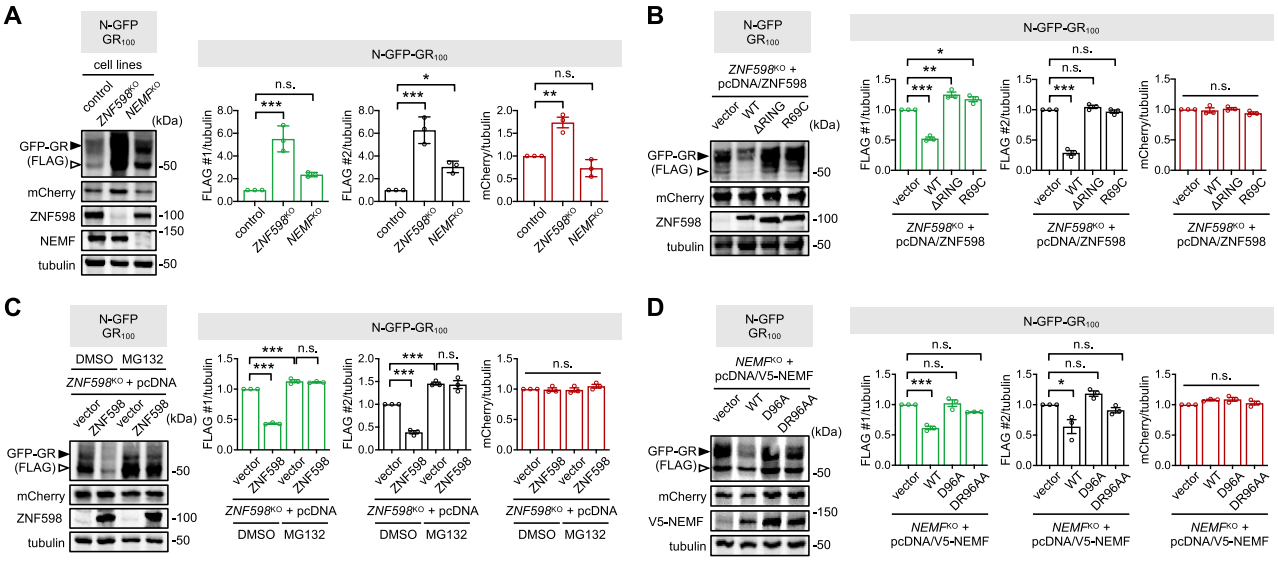

Figure 5. ZNF598 down-regulates poly(GR) expression in a manner distinct from canonical RQC activity. (**A**) Genomic deletion of *ZNF598* or *NEMF* promotes the N-GFP-GR_{100} reporter expression. Control, $ZNF598^{KO}$ and $NEMF^{KO}$ cells were transfected with an expression vector for the N-GFP-GR_{100} reporter. Reporter protein expression was analyzed by immunoblotting with the indicated antibodies. The band intensities for individual reporter proteins were measured and normalized to that for tubulin in each genetic background. Slow- and fast-migrating bands for N-GFP-GR protein were individually quantified as FLAG #1 (black arrowhead) and FLAG #2 (white arrowhead), respectively. The relative levels of individual reporter proteins were then calculated by normalizing to control (set as 1). Data represent means ± SEM ($n = 3$). n.s., not significant; $^{*}P < 0.05$, $^{**}P < 0.01$, $^{***}P < 0.001$, as determined by one-way ANOVA with Dunnett's multiple comparisons test. (**B**) ZNF598 overexpression selectively reduces the expression levels of poly(GR) protein from the N-GFP-GR_{100} reporter. $ZNF598^{KO}$ cells were co-transfected with expression vectors for N-GFP-GR_{100} reporter and ZNF598 protein (wild-type, $ZNF598^{\Delta RING}$ or $ZNF598^{R69C}$). Data represent means ± SEM ($n = 3$). n.s., not significant; $^{*}P < 0.05$, $^{**}P < 0.01$, $^{***}P < 0.001$, as determined by one-way ANOVA with Dunnett's multiple comparisons test. (**C**) Proteasome inhibition blocks ZNF598-dependent downregulation of poly(GR) expression. $ZNF598^{KO}$ cells were co-transfected with expression vectors for N-GFP-GR_{100} reporter and ZNF598 protein. Where indicated, transfected cells were incubated with the proteasome inhibitor MG132 (20 μM) or DMSO (vehicle control) 12 h before harvesting. Two-way ANOVA detected significant interaction effects of ZNF598 overexpression with MG132 treatment on poly(GR) expression ($P < 0.0001$ for FLAG #1; $P = 0.0003$ for FLAG #2). Data represent means ± SEM ($n = 3$). n.s., not significant; $^{***}P < 0.001$, as determined by Tukey's multiple comparisons test. (**D**) NEMF overexpression selectively reduces the expression levels of poly(GR) protein from the N-GFP-GR_{100} reporter. $NEMF^{KO}$ cells were co-transfected with expression vectors for N-GFP-GR_{100} reporter and NEMF protein (wild-type, $NEMF^{D96A}$ or $NEMF^{DR96AA}$). Data represent means ± SEM ($n = 3$). n.s., not significant; $^{*}P < 0.05$, $^{***}P < 0.001$, as determined by one-way ANOVA with Dunnett's multiple comparisons test.

of poly(GR) proteins. We note that long-term treatment of dimethyl sulfoxide (DMSO), a vehicle control for the proteasome inhibitor, somehow elevated the relative levels of fast-migrating poly(GR) protein. Overexpression of wild-type NEMF also suppressed poly(GR) expression in $NEMF^{KO}$ cells (Figure 5D). NEMF variants defective for CAT-tailing activity (i.e. $NEMF^{D96A}$ and $NEMF^{DR96AA}$) displayed no differential effects on the levels of slow- and fast-migrating poly(GR) proteins, contrasting with their specific effects on CAT-tailed RQC substrates (48). We reason that these NEMF mutants may have additional loss-of-function effects.

Interestingly, some phenotypic differences were evident between N-GFP-GR_{100} and N-GFP-$K(AAA)_{20}$ reporters. First, *ZNF598* deletion suppressed the generation of fast-migrating AP from the N-GFP-$K(AAA)_{20}$ reporter (Supplementary Figure S10), whereas ZNF598 overexpression caused more AP generation from the canonical RQC substrate (Supplementary Figure S11). Second, ZNF598 overexpression reduced GFP-K_{20} and mCherry expression (Supplementary Figure S11), but it negligibly affected mCherry expression from the N-GFP-GR_{100} reporter (Figure 5B). On the other hand, NEMF overexpression had relatively specific effects on the fast-migrating AP from the N-GFP-$K(AAA)_{20}$ reporter (Supplementary Figure S12), comparable to those on the slow- and fast-migrating poly(GR) proteins (Figure 5D). We thus hypothesized that the NEMF-LTN1 pathway would recognize intermediates from poly(GR) translation as an RQC substrate for ubiquitin-proteasome degradation, but ZNF598 might play a substrate-specific role in this process (see Discussion section).

ZNF598 promotes ubiquitin-dependent poly(GR) degradation via LTN1-dependent pathway

The canonical RQC pathway removes nascent polypeptides from the 60S subunit after the dissociation of stalled ribosomes. The ubiquitin-dependent proteasomal pathway subsequently degrades translation intermediates. The 60S-associating E3 ligase activity of LTN1 and its ribosomal adaptor protein NEMF mediate this co-translational process (28,39,40). We indeed found that LTN1 overexpression reduced the levels of both slow- and fast-migrating poly(GR) proteins in $LTN1^{KO}$ cells (Figure 6A), but it did not affect mCherry expression, consistent with *NEMF* effects (Figure 5D). This activity required the LTN1 RING domain important for E3 ligase function. To further validate the RQC-relevant poly(GR) regulation, we depleted LTN1 in either control or $ZNF598^{KO}$ cells and examined

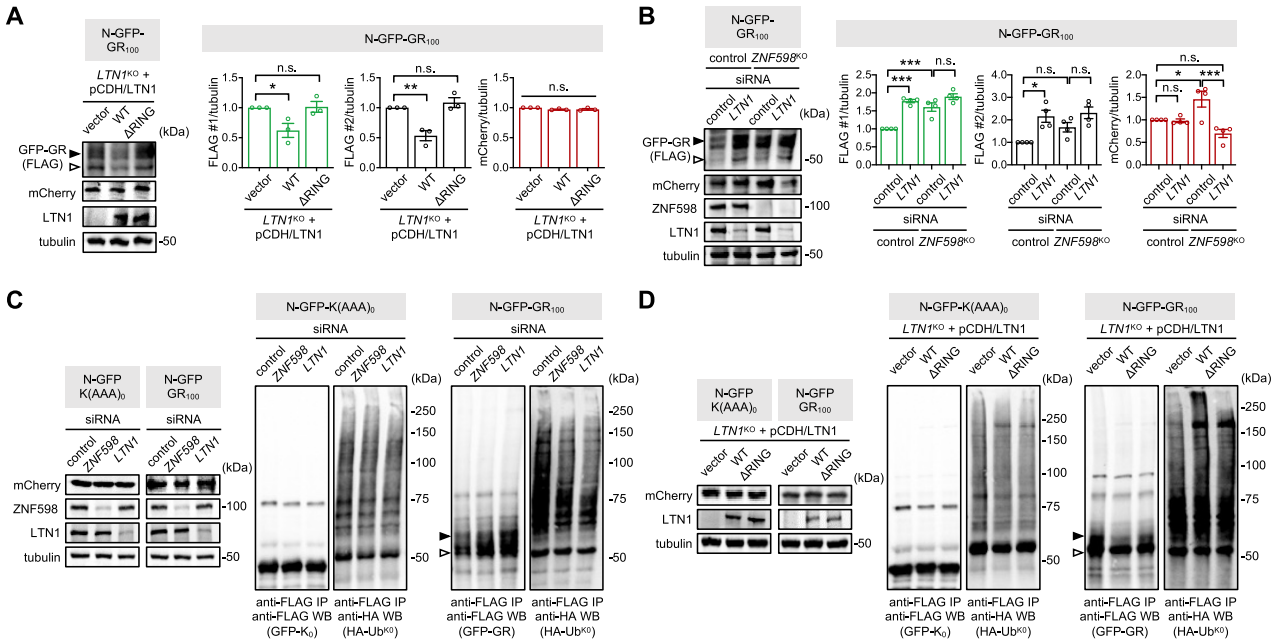

Figure 6. ZNF598 promotes ubiquitin-dependent poly(GR) degradation via the LTN1-dependent pathway. (**A**) LTN1 overexpression selectively reduces the expression levels of poly(GR) protein from the N-GFP-GR$_{100}$ reporter. *LTN1*^{KO} cells were co-transfected with expression vectors for N-GFP-GR$_{100}$ reporter and LTN1 protein (wild-type or LTN1$^{\Delta RING}$). Reporter protein expression was analyzed by immunoblotting and quantified as in Figure 5. Slow- and fast-migrating bands for N-GFP-GR protein were indicated by black (FLAG #1) and white (FLAG #2) arrowheads, respectively. Data represent means ± SEM ($n = 3$). n.s., not significant; *$P < 0.05$, **$P < 0.01$, as determined by one-way ANOVA with Dunnett's multiple comparisons test. (**B**) LTN1 depletion promotes poly(GR) expression non-additively with *ZNF598* deletion. Control and *ZNF598*^{KO} cells were transfected with control^{siRNA} or *LTN1*^{siRNA}. Twelve hours after siRNA transfection, cells were further transfected with an expression vector for the N-GFP-GR$_{100}$ reporter. Two-way ANOVA detected significant interaction effects of LTN1 depletion with *ZNF598* deletion on N-GFP-GR expression ($P = 0.0068$ for FLAG #1; $P = 0.2494$ for FLAG #2). Data represent means ± SEM (n = 4). n.s., not significant; *$P < 0.05$, ***$P < 0.001$, as determined by Tukey's multiple comparisons test. (**C**) Depletion of ZNF598 or LTN1 reduces the polyubiquitination levels of poly(GR) protein. SH-SY5Y cells were sequentially transfected with the indicated siRNA and expression vectors for each translation reporter (N-GFP-K(AAA)$_0$ or N-GFP-GR$_{100}$) and HA-tagged lysine-less ubiquitin protein (HA-Ub^{K0}). Expression of mCherry, ZNF598 and LTN1 was confirmed in soluble cell lysates. The GFP-fusion proteins were further affinity-purified using anti-FLAG antibody under high-stringency conditions and immunoblotted with the indicated antibodies. (**D**) LTN1 overexpression elevates the levels of high-molecular-weight signals for polyubiquitination in poly(GR) protein. *LTN1*^{KO} cells were co-transfected with expression vectors for each translation reporter (N-GFP-K(AAA)$_0$ or N-GFP-GR$_{100}$), HA-Ub^{K0} and LTN1 protein (wild-type or LTN1$^{\Delta RING}$). LTN1-dependent ubiquitination signals in N-GFP-GR protein were assessed similarly as above.

its effects on the translation reporter expression. LTN1 depletion elevated the levels of both slow- and fast-migrating poly(GR) proteins in control cells, but it did not further increase high poly(GR) levels in *ZNF598*^{KO} cells (Figure 6B), suggesting their common genetic pathway for poly(GR) regulation. On the other hand, *ZNF598* effects on mCherry levels were rather suppressed by LTN1 depletion. We confirmed that LTN1 specifically down-regulated AP generation from the N-GFP-K(AAA)$_{20}$ reporter (Supplementary Figures S13 and S14), comparable to its effects on poly(GR) expression. However, the non-additive interplay between ZNF598 and LTN1 was somewhat distinguishable between N-GFP-GR$_{100}$ and N-GFP-K(AAA)$_{20}$ reporters since *ZNF598* deletion abolished AP generation from the N-GFP-K(AAA)$_{20}$ reporter in both control and LTN1-depleted cells (Supplementary Figure S14).

To examine if the ribosome-associated E3 ligases ZNF598 and LTN1 contribute to poly(GR) ubiquitination, we immuno-purified poly(GR) proteins under high-stringency conditions and assessed their ubiquitin signals using immunoblotting. We employed lysine-less ubiquitin (Ub^{K0}) that lacked all of its lysine residues (56,69) and partially blocked ZNF598-dependent degradation of poly(GR) proteins (Supplementary Figure S15). Consequently, co-expression of the epitope-tagged Ub^{K0} allowed us to detect polyubiquitinated poly(GR) proteins more readily. Depletion of ZNF598 or LTN1 indeed reduced the polyubiquitin signals in poly(GR) proteins but not in control reporter proteins (Figure 6C). Furthermore, overexpression of wild-type LTN1, but not of the RING-deletion mutant (i.e. LTN1$^{\Delta RING}$), led to the accumulation of high-molecular-weight signals for polyubiquitination in poly(GR) proteins (Figure 6D). These results support that ZNF598 and LTN1 promote ubiquitin-dependent poly(GR) degradation.

ZNF598 co-translationally titrates poly(GR) expression

To determine if ZNF598-dependent control of poly(GR) expression occurs co-translationally or post-translationally, we first examined the biochemical association of poly(GR) protein with ZNF598 and other RQC factors. Co-immunoprecipitation experiments revealed that the GFP-fusion translation product from the N-GFP-GR$_{100}$ reporter, but not from the other GFP-DPR reporters, formed protein complexes with ZNF598, NEMF and LTN1 proteins (Figure 7A). Moreover, the N-GFP-GR$_{100}$

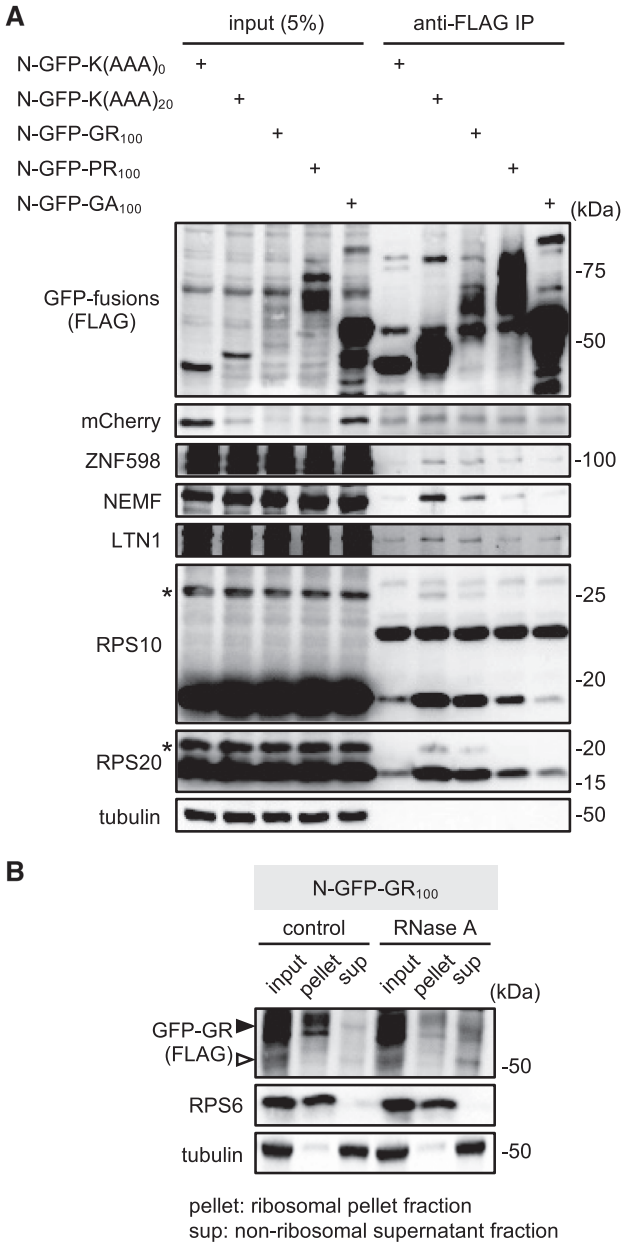

Figure 7. Poly(GR) protein biochemically associates with RQC factors and ribosomes. (**A**) Translation products from N-GFP-K(AAA)$_{20}$ and N-GFP-GR$_{100}$ reporters associate with ZNF598, LTN1, NEMF and two small ribosomal subunit proteins (RPS10 and RSP20) that are ubiquitinated by ZNF598. SH-SY5Y cells were transfected with an expression vector for each translation reporter. Soluble cell lysates were prepared 48 h after transfection and then immunoprecipitated with anti-FLAG antibody. Purified immunoprecipitation (IP) complexes were resolved by SDS-PAGE and immunoblotted with specific antibodies (left). Asterisks, ubiquitinated RPS proteins; input, 5% of soluble extracts used in each IP. (**B**) Poly(GR) protein expressed from the N-GFP-GR$_{100}$ reporter co-sediments with ribosomes in a RNA-dependent manner. SH-SY5Y cells were transfected with an expression vector for N-GFP-GR$_{100}$ reporter. Cell lysates were sedimented by ultracentrifugation in a 35% sucrose cushion. Protein samples were precipitated individually from ribosomal pellet and non-ribosomal supernatant fractions and analyzed by immunoblotting with specific antibodies (left). Where indicated, 100 μg/ml of RNase A was added to the lysate and cushion buffer. Slow- and fast-migrating bands for N-GFP-GR protein were indicated by black and white arrowheads, respectively.

complex included ubiquitinated forms of RPS10 and RPS20 that are targeted by ZNF598 upon ribosomal collisions. The translation product from the canonical RQC substrate (i.e. N-GFP-K(AAA)$_{20}$ reporter) was comparably associated with RQC factors and the two ribosomal proteins (Figure 7A).

Biochemical fractionation using a sucrose cushion showed that RNase treatment reduced the ribosomal association of slow-migrating poly(GR) proteins while increasing the non-ribosomal levels of fast-migrating poly(GR) proteins (Figure 7B). These observations support the idea that poly(GR) protein may associate with the 60S ribosomal subunit as the peptidyl-tRNA conjugate, comparably to other RQC substrates (70,71). Nonetheless, we do not exclude the possibility of RQC-independent interactions between poly(GR) protein and ribosomes (see Discussion).

We further fractionated ribosomes and ribosome-associated proteins from cell extracts using sucrose density-gradient centrifugation and profiled the relative distribution of translation products from the N-GFP-GR$_{100}$ reporter. The standard 10–50% sucrose density gradient showed N-GFP-GR$_{100}$ protein across the 40S and 60S/80S ribosomal fractions (Supplementary Figure S16), whereas N-GFP-K(AAA)$_0$ protein was largely enriched in a lighter non-ribosomal fraction. To obtain a better resolution of the N-GFP-GR$_{100}$ profile over the 40S, 60S, and 80S ribosomal fractions, we employed a 10–40% sucrose density gradient with a modified centrifugation setting and compared N-GFP-GR$_{100}$ profiles at different *ZNF598* gene dosages. N-GFP-GR$_{100}$ protein expressed in *ZNF598*^{KO} cells showed strong co-fractionation with the 40S and 60S ribosomal subunits (Supplementary Figure S17), possibly indicating a ZNF598-independent association (68,72–74). Nonetheless, ZNF598 overexpression significantly reduced the 60S-associating N-GFP-GR$_{100}$ levels, whereas the 40S association of the N-GFP-GR$_{100}$ protein was relatively insensitive to *ZNF598* dosage. We further found that ZNF598^{R69C} overexpression did not significantly affect the 40S- or 60S-associating N-GFP-GR$_{100}$ levels but elevated N-GFP-GR$_{100}$ levels in the 80S ribosomal fraction. These data support a model that ZNF598 senses poly(GR) expression in the context of 80S ribosomes and co-translationally titrates poly(GR) expression. Any residual RQC activity of ZNF598^{R69C} protein may delay this process, leading to the accumulation of poly(GR) protein in the 80S fraction. On the other hand, we reason that lack of ZNF598 protein facilitates the escape of poly(GR) protein from the 80S-associated RQC while a substantial portion of those 'escapees' likely remains associated with ribosomal subunits.

ZNF598 overexpression suppresses poly(GR) expression and proapoptotic activation in C9-ALS patient-derived neurons

The initiation rate of the RAN translation is thought to be much lower than that of AUG-initiated general translation. This difference could affect the density of translating ribosomes on a given mRNA and thereby the probability of ribosomal collisions that might trigger RQC activity. Since all our transgenic reporters were based on the AUG-initiated

translation for poly(GR) expression, we asked if ZNF598 would display similar effects on the RAN translation-dependent expression of poly(GR) protein from pathogenic hexanucleotide repeats in ALS-associated *C9ORF72* loci. To this end, we employed induced pluripotent stem cells from *C9ORF72*-associated ALS patients (C9-ALS iPSCs; CS28, CS29 and CS52 lines) along with a group of control iPSCs (CS0, CS29-ISO and CS4 lines) and differentiated them into motor neurons. These iPSC-derived neuron cultures (i.e. C9-ALS iPSNs and control iPSNs) included an isogenic pair (i.e. CS29 and CS29-ISO) where ∼800 hexanucleotide repeats in the ALS-associated *C9ORF72* locus were deleted by the CRISPR/Cas9-mediated genome editing (75). We then performed a series of experiments to validate the physiological relevance of ZNF598 to cellular pathologies in C9-ALS iPSNs.

We first found that the baseline RQC activity was impaired in all the three C9-ALS iPSN cultures when assessed by the lentiviral reporter for the canonical RQC substrate (i.e. $K(AAA)_{20}$ reporters) (Figure 8A and B). RQC deficiency in C9-ALS iPSNs was consistent with their low expression of ZNF598 protein, but not of *ZNF598* mRNA, compared to control iPSNs (Supplementary Figure S18). In contrast, we observed high levels of NEMF and LTN1 proteins in C9-ALS iPSNs, suggesting a possible compensation mechanism in the RQC pathway. We hypothesized that ZNF598 overexpression might rescue the RQC activity in C9-ALS iPSNs, lower poly(GR) expression, and suppress neurodegenerative phenotypes. We thus generated recombinant lentiviruses that drive the overexpression of wild-type or mutant ZNF598 along with the transduction marker GFP (Supplementary Figure S19). Of note, our iPSC differentiation led to a heterogenous culture of neurons and non-neuronal cells from the parental iPSC. Moreover, the transduction efficiency of recombinant lentiviruses was not 100% and varied among the iPSN cultures. We reasoned that the heterogeneity of the cell population (e.g. non-neuronal or non-infected cells) could mask true signals in immunological analyses of the whole-culture lysates (e.g. ELISA or dot blot), making their results inconclusive. Accordingly, we stained the heterogenous iPSN cultures with specific-marker antibodies to identify transduced iPSNs and quantified their immunofluorescence signals to assess the transgenic effects of ZNF598 more accurately.

Under our experimental conditions, poly(GR) proteins were readily detectable as cytoplasmic puncta in neurites of C9-ALS iPSNs but not of control iPSNs (Figure 8C). This subcellular pattern of endogenous poly(GR) proteins was distinct from that of transgenic ones in immortalized cell lines, and we reasoned that the post-mitotic nature of iPSNs and much longer repeats in endogenous poly(GR) proteins could explain this difference. Nonetheless, we confirmed that lentiviral overexpression of wild-type ZNF598, but not of RQC-defective ZNF598 mutants ($ZNF598^{\Delta RING}$ or $ZNF598^{R69C}$), significantly reduced the number and size of poly(GR) granules in all C9-ALS iPSNs tested (Figure 8C and D; Supplementary Figure S20), although the lack of $ZNF598^{\Delta RING}$ effects could be due to its weaker expression than wild-type ZNF598 (Supplementary Figure S19). There were no comparable effects of ZNF598 overexpression on the formation of poly(PR) granules in C9-ALS iPSNs (Supplementary Figure S21), consistent with modest RQC effects on poly(PR) in immortalized cell lines (Supplementary Figures S10–S13) and transgenic flies (Figure 1C). Importantly, ZNF598 overexpression also reduced the percentage of C9-ALS iPSNs expressing cleaved caspase-3 protein (Figure 8E and F; Supplementary Figure S22), an indication of the proapoptotic activation in C9-ALS iPSN cultures (76,77). Taken together, these results support the physiological relevance of ZNF598 to poly(GR) regulation, convincingly defining its neuroprotective role in the pathogenesis of C9-ALS/FTD.

DISCUSSION

Proteostasis is essential for cellular physiology and is sustained by quality control pathways in gene expression. RQC represents a co-translational mechanism that triages aberrant translation intermediates via proteasomal degradation while efficiently recycling translationally stalled ribosomes. We demonstrate that ZNF598, a key player of this molecular surveillance machinery, participates in the co-translational control of ALS-associated poly(GR) protein and suppresses cellular pathologies in ALS patient-derived neurons. Nevertheless, the underlying mechanism has features distinct from ZNF598 activity on the poly-A translation-based RQC reporter. These differences may reflect the adaptive nature and plasticity of the RQC-relevant ZNF598 function that has evolved to co-translationally surveil a myriad of ribosomal events and translational intermediates. Indeed, emerging evidence suggests that the hierarchical operation of ribosome-associating factors triggers differential molecular procedures for co-translational control and downstream signaling pathways, depending on the quality and context of ribosomal collisions (78,79).

Our evidence indicates that ZNF598 and LTN1 together co-translationally titrate poly(GR) expression via the ubiquitin-dependent mechanism. Comparable effects of the NEMF-LTN1 pathway on poly(GR) protein and GFP-$K(AAA)_{20}$-derived AP suggest that they serve as equivalent RQC substrates. However, genetic manipulations of the *ZNF598* dosage led to puzzling effects on the two translationally stalling products and downstream translation, revealing the diversity of RQC mechanisms via the substrate-specific ZNF598 function. *ZNF598* deletion promoted both expressions of poly(GR) and downstream mCherry from the N-GFP-GR_{100} reporter, whereas ZNF598 overexpression lowered the poly(GR) levels only. Considering that ribosomal stalling cues other translation regulators to block additional translation initiation on the given mRNA molecule (80–82), *ZNF598* deletion may de-repress this feedback inhibition on the N-GFP-GR_{100} reporter and enhance its overall translation. We further reason that the translation repressor complex might be limiting in ZNF598-overexpressing cells since the overexpression phenotypes were primarily detected on the co-translational degradation of poly(GR) protein. On the other hand, *ZNF598* effects on the N-GFP-$K(AAA)_{20}$ reporter likely involve an RNA-dependent mechanism, and ZNF598 overexpression may promote the reporter RNA decay (83), thereby suppressing both N-GFP-K_{20} and mCherry expression. LTN1 depletion also displayed some interesting phenotypes, depending

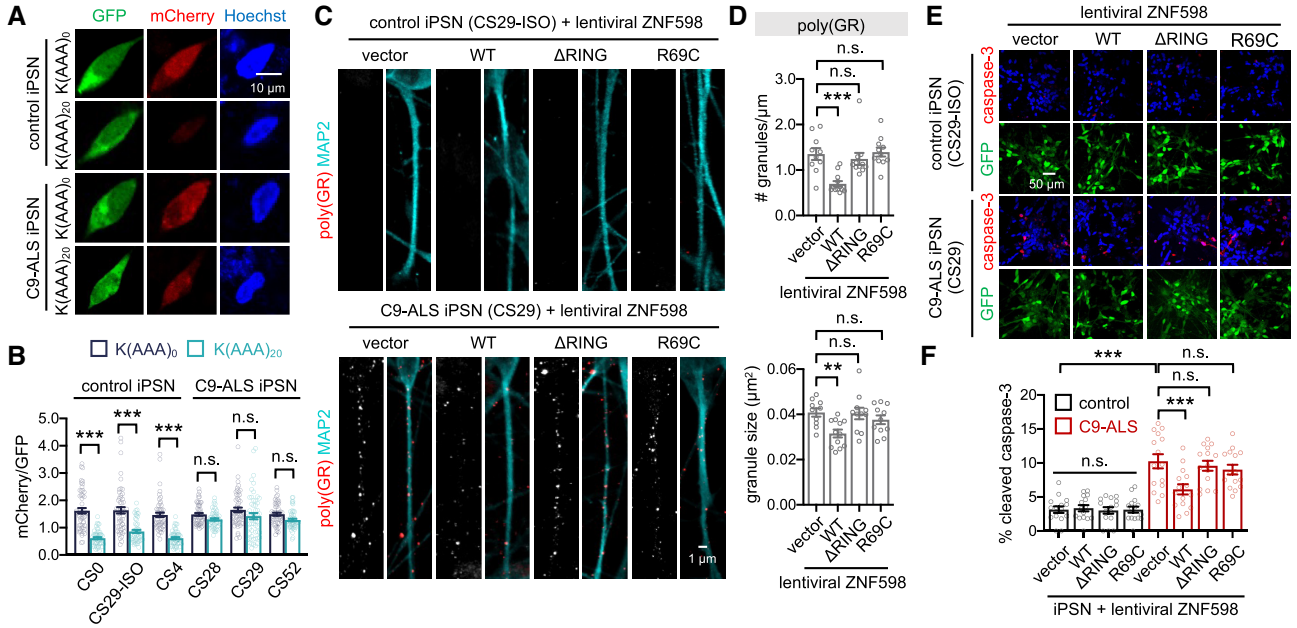

Figure 8. ZNF598 suppresses poly(GR) expression and proapoptotic activation in C9-ALS patient-derived neurons. (**A** and **B**) C9-ALS iPSNs display no translational stalling on the canonical RQC substrate $K(AAA)_{20}$. Individual NPCs from control iPSC lines (CS0, CS29-ISO, and CS4 lines) and C9-ALS iPSC lines (CS28, CS29 and CS52 lines) were transduced with recombinant lentiviruses that express $K(AAA)_0$ or $K(AAA)_{20}$ translation reporter. Control and C9-ALS iPSN cultures were fixed one week after neuronal differentiation from the NPCs and stained with Hoechst 33258 (blue). Translational stalling was quantified by the ratio of mCherry to GFP fluorescence in individual cells. Data represent means ± SEM (n = 52–53 cells from three independent differentiation experiments). n.s., not significant; $^{***}P < 0.001$, as determined by two-way ANOVA with Tukey's multiple comparisons test. (**C** and **D**) ZNF598 overexpression suppresses the formation of poly(GR) granules in C9-ALS iPSNs. NPCs from C9-ALS iPSCs (CS29 line) and their isogenic control iPSCs (CS29-ISO line) were transduced with recombinant lentiviruses that express the indicated ZNF598 proteins along with the transduction reporter GFP. Control and C9-ALS iPSN cultures were fixed one week after neuronal differentiation from the NPCs and co-stained with anti-MAP2 antibody (cyan) and anti-poly(GR) antibody (red). The number of poly(GR) granules per MAP2–positive neurite and their sizes were quantified in C9-ALS iPSNs (CS29 line) using ImageJ software and averaged (n = 10–12 GFP–positive neurons from three independent differentiation experiments). Error bars indicate SEM. n.s., not significant; $^{**}P < 0.01$, $^{***}P < 0.001$, as determined by one-way ANOVA with Dunnett's multiple comparisons test. (**E** and **F**) ZNF598 overexpression suppresses caspase-3 activation in C9-ALS iPSNs. Three-week-old C9-ALS iPSNs (CS29 line) and their isogenic control neurons (CS29-ISO line) were co-stained with anti-cleaved caspase-3 antibody (red), anti-MAP2 antibody, and Hoechst 33258 (blue). The relative percentages of iPSNs expressing cleaved caspase-3 were averaged from 15 confocal images of random fields of interest per condition (n = 712–826 GFP–positive neurons from three independent differentiation experiments). Data represent means ± SEM. n.s., not significant; $^{***}P < 0.001$, as determined by two-way ANOVA with Tukey's post hoc test.

on *ZNF598* gene dosage and translation reporters. ZNF598 acted upstream of LTN1 on the N-GFP-$K(AAA)_{20}$ reporter since ZNF598 was necessary for AP generation from poly-A translation and *ZNF598* deletion blocked *LTN1* effects on the AP generation and downstream mCherry expression. By contrast, poly(GR) expression was promoted by non-additive effects of *ZNF598* deletion and LTN1 depletion. *ZNF598* deletion failed to enhance mCherry expression downstream of the poly(GR) translation in LTN1-depleted cells, suggesting a possible role of LTN1 in translational effects of *ZNF598* deletion.

How does ZNF598 display substrate-specific effects in RQC function? We reason that the molecular context of translational stalling will determine the mode of ZNF598 action on individual RQC substrates, explaining the phenotypic difference between N-GFP-GR_{100} and N-GFP-$K(AAA)_{20}$ reporters. Ribosomal collisions during poly-A translation may impose the rate-limiting function of ZNF598 on ribosomal disassembly that generates AP and suppresses downstream translation. Codon-independent effects of the poly(GR)-encoding sequences on translation elongation suggest that the translation products of alternating arginine residues, but not their decoding process per se, are likely responsible for translational stalling. In fact, electrostatic interactions between the positively charged nascent chain and negatively charged ribosomal RNA should delay the extrusion of translation products from ribosomes and slow down the translational elongation by individual ribosomes (84,85). Previous studies have also shown a biochemical association of arginine-containing DPR proteins with ribosomal proteins (68,72–74), although it is unclear whether their interaction is the cause or effect of translational stalling. We speculate that this translational context would make ribosomal stalling on poly(GR)-encoding mRNAs less sensitive to the ZNF598 dosage. Instead, ZNF598 may play more prominent roles in facilitating the LTN1-dependent clearance of translation intermediates or blocking additional ribosome loading onto the given mRNA for relieving a translational burden.

Evidence for the involvement of co-translational quality control in neurodegeneration has recently emerged. Neurodegenerative phenotypes have been documented in *Ltn1* mutant mice (86), and a deficiency of *ltn1*-dependent RQC induces proteotoxic stress in yeast (87). These observations are consistent with motor neuron degeneration in *Nemf* mutant mice and *NEMF* association with human neuro-

muscular disease (88). Mutations in a CNS-specific tRNA and GTPBP2, a translational GTPase that interacts with the ribosome-recycling factor PELOTA, induces ribosomal stalling on a specific codon (i.e. AGA) and leads to age-dependent neurodegeneration in mice (89). Mitochondrial dysfunction also promotes non-templated C-terminal extensions of translation products by CAT-tailing, and co-translational quality control factors suppress their toxic expression in Parkinson's disease models (90). Our study illustrates how the key RQC factor ZNF598 could act as a molecular suppressor specific to C9-ALS/FTD, among other neurodegenerative disorders.

In fact, co-translational mRNA surveillance mechanisms have been implicated in C9-ALS pathogenesis, and it has been shown that *C9ORF72* mRNA is a substrate of NMD (91). However, evidence for NMD activity in C9-ALS is conflicting. The genetic conditions of NMD deficiency and C9-ALS share an overlapping gene expression profile (65). Transgenic overexpression of DPR proteins in cultured cells inhibits NMD, likely via the subcellular transition of the RNA-decaying P-body to stress granule. On the other hand, C9-ALS iPSNs display high rather than low NMD activity, an effect that is likely mediated by switching eRF1-dependent function from translation termination to UPF1-dependent NMD (91). In either case, genetic or pharmacological activation of NMD ameliorates cytotoxicity related to C9-ALS, supporting its neuroprotective role. The relevance of the UPF1-dependent mRNA surveillance pathway, however, is not limited to this specific type of ALS since UPF1 also modulates TDP-43 and FUS toxicity associated with ALS pathogenesis (92–95).

Taken together, we propose that the ribosome-associated E3 ligases ZNF598 and LTN1 constitute an innate molecular defense that limits the atypical translation of pathogenic poly(GR) protein implicated in C9-ALS/FTD pathogenesis. Our findings broaden the known repertoire of RQC-relevant physiology while being complementary to an independent study implicating CAT-tailing-like modification of poly(GR) protein in its clearance by mitochondria-associated RQC (96). Future studies should elucidate how RQC mechanisms intimately cooperate with RNA quality control pathways and translational machinery. It will also be important to understand how the RQC pathway interacts with the progress of C9-ALS/FTD for developing therapeutic opportunities.

DATA AVAILABILITY

All relevant data are included in the published paper and Supplementary Data file. Raw data are available from the corresponding author upon request.

SUPPLEMENTARY DATA

Supplementary Data are available at NAR Online.

ACKNOWLEDGEMENTS

We thank R.S. Hegde, T. Inada, D. Ito, L.P.W. Ranum, J.D. Rothstein, Addgene, Bloomington *Drosophila* Stock Center, Korea *Drosophila* Resource Center, National Institute of Genetics, Cedars-Sinai iPSC Core, and Vienna *Drosophila* Resource Center for reagents; H. Joung and J.-H. Hur at UNIST Optical Biomed Imaging Center for technical assistance in confocal imaging.

FUNDING

Suh Kyungbae Foundation [SUHF-17020101]; National Research Foundation, Republic of Korea [NRF-2018R1A2B2004641, NRF-2018R1A5A1024261, NRF-2021R1A2C3011706, NRF-2021M3A9G8022960]. Funding for open access charge: Suh Kyungbae Foundation [SUHF-17020101].
Conflict of interest statement. None declared.

REFERENCES

1. Balendra,R. and Isaacs,A.M. (2018) C9orf72-mediated ALS and FTD: multiple pathways to disease. *Nat. Rev. Neurol.*, **14**, 544–558.
2. Gao,F.B., Almeida,S. and Lopez-Gonzalez,R. (2017) Dysregulated molecular pathways in amyotrophic lateral sclerosis-frontotemporal dementia spectrum disorder. *EMBO J.*, **36**, 2931–2950.
3. DeJesus-Hernandez,M., Mackenzie,I.R., Boeve,B.F., Boxer,A.L., Baker,M., Rutherford,N.J., Nicholson,A.M., Finch,N.A., Flynn,H., Adamson,J. *et al.* (2011) Expanded GGGGCC hexanucleotide repeat in noncoding region of C9ORF72 causes chromosome 9p-linked FTD and ALS. *Neuron*, **72**, 245–256.
4. Gijselinck,I., Van Langenhove,T., van der Zee,J., Sleegers,K., Philtjens,S., Kleinberger,G., Janssens,J., Bettens,K., Van Cauwenberghe,C., Pereson,S. *et al.* (2012) A C9orf72 promoter repeat expansion in a Flanders-Belgian cohort with disorders of the frontotemporal lobar degeneration-amyotrophic lateral sclerosis spectrum: a gene identification study. *Lancet Neurol.*, **11**, 54–65.
5. Renton,A.E., Majounie,E., Waite,A., Simón-Sánchez,J., Rollinson,S., Gibbs,J.R., Schymick,J.C., Laaksovirta,H., van,Swieten, John,C., Myllykangas,L. *et al.* (2011) A hexanucleotide repeat expansion in C9ORF72 is the cause of chromosome 9p21-linked ALS-FTD. *Neuron*, **72**, 257–268.
6. Gitler,A.D. and Tsuiji,H. (2016) There has been an awakening: emerging mechanisms of C9orf72 mutations in FTD/ALS. *Brain Res.*, **1647**, 19–29.
7. Gendron,T.F. and Petrucelli,L. (2018) Disease mechanisms of C9ORF72 repeat expansions. *Cold Spring Harb. Perspect. Med.*, **8**, a024224.
8. Ash,P.E., Bieniek,K.F., Gendron,T.F., Caulfield,T., Lin,W.L., Dejesus-Hernandez,M., van Blitterswijk,M.M., Jansen-West,K., Paul,J.W. 3rd, Rademakers,R. *et al.* (2013) Unconventional translation of C9ORF72 GGGGCC expansion generates insoluble polypeptides specific to c9FTD/ALS. *Neuron*, **77**, 639–646.
9. Mori,K., Weng,S.M., Arzberger,T., May,S., Rentzsch,K., Kremmer,E., Schmid,B., Kretzschmar,H.A., Cruts,M., Van Broeckhoven,C. *et al.* (2013) The C9orf72 GGGGCC repeat is translated into aggregating dipeptide-repeat proteins in FTLD/ALS. *Science*, **339**, 1335–1338.
10. Zu,T., Liu,Y., Bañez-Coronel,M., Reid,T., Pletnikova,O., Lewis,J., Miller,T.M., Harms,M.B., Falchook,A.E., Subramony,S.H. *et al.* (2013) RAN proteins and RNA foci from antisense transcripts in *C9ORF72* ALS and frontotemporal dementia. *Proc. Natl. Acad. Sci.*, **110**, E4968–E4977.
11. Boeynaems,S., Bogaert,E., Michiels,E., Gijselinck,I., Sieben,A., Jovicic,A., De Baets,G., Scheveneels,W., Steyaert,J., Cuijt,I. *et al.* (2016) Drosophila screen connects nuclear transport genes to DPR pathology in c9ALS/FTD. Sci. Rep., **6**, 20877.
12. Jovičić,A., Mertens,J., Boeynaems,S., Bogaert,E., Chai,N., Yamada,S.B., Paul,J.W. 3rd, Sun,S., Herdy,J.R., Bieri,G. *et al.* (2015) Modifiers of C9orf72 dipeptide repeat toxicity connect nucleocytoplasmic transport defects to FTD/ALS. *Nat. Neurosci.*, **18**, 1226–1229.
13. Kramer,N.J., Haney,M.S., Morgens,D.W., Jovicic,A., Couthouis,J., Li,A., Ousey,J., Ma,R., Bieri,G., Tsui,C.K. *et al.* (2018) CRISPR-Cas9 screens in human cells and primary neurons identify modifiers of C9ORF72 dipeptide-repeat-protein toxicity. *Nat. Genet.*, **50**, 603–612.

14. Zhang,K., Daigle,J.G., Cunningham,K.M., Coyne,A.N., Ruan,K., Grima,J.C., Bowen,K.E., Wadhwa,H., Yang,P., Rigo,F. *et al.* (2018) Stress granule assembly disrupts nucleocytoplasmic transport. Cell, **173**, 958–971.
15. Zhang,K., Donnelly,C.J., Haeusler,A.R., Grima,J.C., Machamer,J.B., Steinwald,P., Daley,E.L., Miller,S.J., Cunningham,K.M., Vidensky,S. *et al.* (2015) The C9orf72 repeat expansion disrupts nucleocytoplasmic transport. *Nature*, **525**, 56–61.
16. Hayes,L.R., Duan,L., Bowen,K., Kalab,P. and Rothstein,J.D. (2020) C9orf72 arginine-rich dipeptide repeat proteins disrupt karyopherin-mediated nuclear import. *Elife*, **9**, e51685.
17. Freibaum,B.D., Lu,Y., Lopez-Gonzalez,R., Kim,N.C., Almeida,S., Lee,K.H., Badders,N., Valentine,M., Miller,B.L., Wong,P.C. *et al.* (2015) GGGGCC repeat expansion in C9orf72 compromises nucleocytoplasmic transport. *Nature*, **525**, 129–133.
18. Lee,J., Park,J., Kim,J.H., Lee,G., Park,T.E., Yoon,K.J., Kim,Y.K. and Lim,C. (2020) LSM12-EPAC1 defines a neuroprotective pathway that sustains the nucleocytoplasmic RAN gradient. *PLoS Biol.*, **18**, e3001002.
19. Fallini,C., Khalil,B., Smith,C.L. and Rossoll,W. (2020) Traffic jam at the nuclear pore: All roads lead to nucleocytoplasmic transport defects in ALS/FTD. *Neurobiol. Dis.*, **140**, 104835.
20. Yuva-Aydemir,Y., Almeida,S. and Gao,F.-B. (2018) Insights into *C9ORF72*-Related ALS/FTD from *Drosophila* and iPSC Models. *Trends Neurosci.*, **41**, 457–469.
21. Freibaum,B.D. and Taylor,J.P. (2017) The role of dipeptide repeats in C9ORF72-related ALS-FTD. *Front. Mol. Neurosci.*, **10**, 35.
22. Simms,C.L., Thomas,E.N. and Zaher,H.S. (2017) Ribosome-based quality control of mRNA and nascent peptides. *Wiley Interdiscip. Rev. RNA*, **8**, e1366.
23. Shoemaker,C.J. and Green,R. (2012) Translation drives mRNA quality control. *Nat. Struct. Mol. Biol.*, **19**, 594–601.
24. Collart,M.A. and Weiss,B. (2020) Ribosome pausing, a dangerous necessity for co-translational events. *Nucleic Acids Res.*, **48**, 1043–1055.
25. Ikeuchi,K., Izawa,T. and Inada,T. (2018) Recent progress on the molecular mechanism of quality controls induced by ribosome stalling. *Front Genet*., **9**, 743.
26. Inada,T. (2020) Quality controls induced by aberrant translation. *Nucleic Acids Res.*, **48**, 1084–1096.
27. Joazeiro,C.A.P. (2019) Mechanisms and functions of ribosome-associated protein quality control. *Nat. Rev. Mol. Cell Biol.*, **20**, 368–383.
28. Brandman,O., Stewart-Ornstein,J., Wong,D., Larson,A., Williams,C.C., Li,G.W., Zhou,S., King,D., Shen,P.S., Weibezahn,J. *et al.* (2012) A ribosome-bound quality control complex triggers degradation of nascent peptides and signals translation stress. *Cell*, **151**, 1042–1054.
29. Brandman,O. and Hegde,R.S. (2016) Ribosome-associated protein quality control. *Nat. Struct. Mol. Biol.*, **23**, 7–15.
30. Letzring,D.P., Wolf,A.S., Brule,C.E. and Grayhack,E.J. (2013) Translation of CGA codon repeats in yeast involves quality control components and ribosomal protein L1. *RNA*, **19**, 1208–1217.
31. Saito,K., Horikawa,W. and Ito,K. (2015) Inhibiting K63 polyubiquitination abolishes no-go type stalled translation surveillance in Saccharomyces cerevisiae. *PLoS Genet.*, **11**, e1005197.
32. Juszkiewicz,S. and Hegde,R.S. (2017) Initiation of quality control during poly(A) translation requires site-specific ribosome ubiquitination. *Mol. Cell*, **65**, 743–750.
33. Sundaramoorthy,E., Leonard,M., Mak,R., Liao,J., Fulzele,A. and Bennett,E.J. (2017) ZNF598 and RACK1 regulate mammalian ribosome-associated quality control function by mediating regulatory 40S ribosomal ubiquitylation. *Mol. Cell*, **65**, 751–760.
34. Garzia,A., Jafarnejad,S.M., Meyer,C., Chapat,C., Gogakos,T., Morozov,P., Amiri,M., Shapiro,M., Molina,H., Tuschl,T. *et al.* (2017) The E3 ubiquitin ligase and RNA-binding protein ZNF598 orchestrates ribosome quality control of premature polyadenylated mRNAs. *Nat. Commun.*, **8**, 16056.
35. Matsuo,Y., Ikeuchi,K., Saeki,Y., Iwasaki,S., Schmidt,C., Udagawa,T., Sato,F., Tsuchiya,H., Becker,T., Tanaka,K. *et al.* (2017) Ubiquitination of stalled ribosome triggers ribosome-associated quality control. *Nat. Commun.*, **8**, 159.
36. Sitron,C.S., Park,J.H. and Brandman,O. (2017) Asc1, Hel2, and Slh1 couple translation arrest to nascent chain degradation. *RNA*, **23**, 798–810.
37. Juszkiewicz,S., Chandrasekaran,V., Lin,Z., Kraatz,S., Ramakrishnan,V. and Hegde,R.S. (2018) ZNF598 Is a quality control sensor of collided ribosomes. *Mol. Cell*, **72**, 469–481.
38. Ikeuchi,K., Tesina,P., Matsuo,Y., Sugiyama,T., Cheng,J., Saeki,Y., Tanaka,K., Becker,T., Beckmann,R. and Inada,T. (2019) Collided ribosomes form a unique structural interface to induce Hel2-driven quality control pathways. *EMBO J.*, **38**, e100276.
39. Bengtson,M.H. and Joazeiro,C.A. (2010) Role of a ribosome-associated E3 ubiquitin ligase in protein quality control. *Nature*, **467**, 470–473.
40. Defenouillere,Q., Yao,Y., Mouaikel,J., Namane,A., Galopier,A., Decourty,L., Doyen,A., Malabat,C., Saveanu,C., Jacquier,A. *et al.* (2013) Cdc48-associated complex bound to 60S particles is required for the clearance of aberrant translation products. *Proc. Natl. Acad. Sci. U. S. A.*, **110**, 5046–5051.
41. Shoemaker,C.J., Eyler,D.E. and Green,R. (2010) Dom34:Hbs1 promotes subunit dissociation and peptidyl-tRNA drop-off to initiate no-go decay. *Science*, **330**, 369–372.
42. Pisareva,V.P., Skabkin,M.A., Hellen,C.U., Pestova,T.V. and Pisarev,A.V. (2011) Dissociation by Pelota, Hbs1 and ABCE1 of mammalian vacant 80S ribosomes and stalled elongation complexes. *EMBO J.*, **30**, 1804–1817.
43. Shao,S., von der Malsburg,K. and Hegde,R.S. (2013) Listerin-dependent nascent protein ubiquitination relies on ribosome subunit dissociation. *Mol. Cell*, **50**, 637–648.
44. Lyumkis,D., Oliveira dos Passos,D., Tahara,E.B., Webb,K., Bennett,E.J., Vinterbo,S., Potter,C.S., Carragher,B. and Joazeiro,C.A. (2014) Structural basis for translational surveillance by the large ribosomal subunit-associated protein quality control complex. *Proc. Natl. Acad. Sci. U.S.A.*, **111**, 15981–15986.
45. Yonashiro,R., Tahara,E.B., Bengtson,M.H., Khokhrina,M., Lorenz,H., Chen,K.C., Kigoshi-Tansho,Y., Savas,J.N., Yates,J.R., Kay,S.A. *et al.* (2016) The Rqc2/Tae2 subunit of the ribosome-associated quality control (RQC) complex marks ribosome-stalled nascent polypeptide chains for aggregation. *Elife*, **5**, e11794.
46. Shen,P.S., Park,J., Qin,Y., Li,X., Parsawar,K., Larson,M.H., Cox,J., Cheng,Y., Lambowitz,A.M., Weissman,J.S. *et al.* (2015) Rqc2p and 60S ribosomal subunits mediate mRNA-independent elongation of nascent chains. *Science*, **347**, 75–78.
47. Thrun,A., Garzia,A., Kigoshi-Tansho,Y., Patil,P.R., Umbaugh,C.S., Dallinger,T., Liu,J., Kreger,S., Patrizi,A., Cox,G.A. *et al.* (2021) Convergence of mammalian RQC and C-end rule proteolytic pathways via alanine tailing. *Mol. Cell*, **81**, 2112–2122.
48. Udagawa,T., Seki,M., Okuyama,T., Adachi,S., Natsume,T., Noguchi,T., Matsuzawa,A. and Inada,T. (2021) Failure to Degrade CAT-Tailed Proteins disrupts neuronal morphogenesis and cell survival. *Cell Rep.*, **34**, 108599.
49. Osuna,B.A., Howard,C.J., Kc,S., Frost,A. and Weinberg,D.E. (2017) In vitro analysis of RQC activities provides insights into the mechanism and function of CAT tailing. *Elife*, **6**, e27949.
50. Kostova,K.K., Hickey,K.L., Osuna,B.A., Hussmann,J.A., Frost,A., Weinberg,D.E. and Weissman,J.S. (2017) CAT-tailing as a fail-safe mechanism for efficient degradation of stalled nascent polypeptides. *Science*, **357**, 414–417.
51. Sitron,C.S. and Brandman,O. (2019) CAT tails drive degradation of stalled polypeptides on and off the ribosome. *Nat. Struct. Mol. Biol.*, **26**, 450–459.
52. Verma,R., Oania,R.S., Kolawa,N.J. and Deshaies,R.J. (2013) Cdc48/p97 promotes degradation of aberrant nascent polypeptides bound to the ribosome. *Elife*, **2**, e00308.
53. Verma,R., Reichermeier,K.M., Burroughs,A.M., Oania,R.S., Reitsma,J.M., Aravind,L. and Deshaies,R.J. (2018) Vms1 and ANKZF1 peptidyl-tRNA hydrolases release nascent chains from stalled ribosomes. *Nature*, **557**, 446–451.
54. Zurita Rendon,O., Fredrickson,E.K., Howard,C.J., Van Vranken,J., Fogarty,S., Tolley,N.D., Kalia,R., Osuna,B.A., Shen,P.S., Hill,C.P. *et al.* (2018) Vms1p is a release factor for the ribosome-associated quality control complex. *Nat. Commun.*, **9**, 2197.
55. Farg,M.A., Konopka,A., Soo,K.Y., Ito,D. and Atkin,J.D. (2017) The DNA damage response (DDR) is induced by the C9orf72 repeat

expansion in amyotrophic lateral sclerosis. *Hum. Mol. Genet.*, **26**, 2882–2896.
56. Lim,K.L., Chew,K.C., Tan,J.M., Wang,C., Chung,K.K., Zhang,Y., Tanaka,Y., Smith,W., Engelender,S., Ross,C.A. *et al.* (2005) Parkin mediates nonclassical, proteasomal-independent ubiquitination of synphilin-1: implications for Lewy body formation. *J. Neurosci.*, **25**, 2002–2009.
57. Cheng,W.W., Wang,S.P., Zhang,Z., Morgens,D.W., Hayes,L.R., Lee,S., Portz,B., Xie,Y.Z., Nguyen,B.V., Haney,M.S. *et al.* (2019) CRISPR-Cas9 Screens Identify the RNA Helicase DDX3X as a Repressor of C9ORF72 (GGGGCC)n Repeat-Associated Non-AUG Translation. *Neuron*, **104**, 885–898.
58. Longo,P.A., Kavran,J.M., Kim,M.S. and Leahy,D.J. (2013) Transient mammalian cell transfection with polyethylenimine (PEI). *Methods Enzymol.*, **529**, 227–240.
59. Garshott,D.M., Sundaramoorthy,E., Leonard,M. and Bennett,E.J. (2020) Distinct regulatory ribosomal ubiquitylation events are reversible and hierarchically organized. *Elife*, **9**, e54023.
60. Han,P., Shichino,Y., Schneider-Poetsch,T., Mito,M., Hashimoto,S., Udagawa,T., Kohno,K., Yoshida,M., Mishima,Y., Inada,T. *et al.* (2020) Genome-wide survey of ribosome collision. *Cell Rep.*, **31**, 107610.
61. Mizielinska,S., Gronke,S., Niccoli,T., Ridler,C.E., Clayton,E.L., Devoy,A., Moens,T., Norona,F.E., Woollacott,I.O.C., Pietrzyk,J. *et al.* (2014) C9orf72 repeat expansions cause neurodegeneration in Drosophila through arginine-rich proteins. *Science*, **345**, 1192–1194.
62. Goodman,L.D., Prudencio,M., Kramer,N.J., Martinez-Ramirez,L.F., Srinivasan,A.R., Lan,M., Parisi,M.J., Zhu,Y.Q., Chew,J., Cook,C.N. *et al.* (2019) Toxic expanded GGGGCC repeat transcription is mediated by the PAF1 complex in C9orf72-associated FTD. *Nat. Neurosci.*, **22**, 863–874.
63. Goodman,L.D., Prudencio,M., Srinivasan,A.R., Rifai,O.M., Lee,V.M.Y., Petrucelli,L. and Bonini,N.M. (2019) eIF4B and eIF4H mediate GR production from expanded G4C2 in a Drosophila model for C9orf72-associated ALS. *Acta Neuropathol. Com.*, **7**, 62.
64. Lee,K.H., Zhang,P.P., Kim,H.J., Mitrea,D.M., Sarkar,M., Freibaum,B.D., Cika,J., Coughlin,M., Messing,J., Molliex,A. *et al.* (2016) C9orf72 dipeptide repeats impair the assembly, dynamics, and function of membrane-less organelles. *Cell*, **167**, 774–788.
65. Xu,W.C., Bao,P.H., Jiang,X., Wang,H.F., Qin,M.L., Wang,R.Q., Wang,T., Yang,Y., Lorenzini,I., Liao,L.J. *et al.* (2019) Reactivation of nonsense-mediated mRNA decay protects against C9orf72 dipeptide-repeat neurotoxicity. *Brain*, **142**, 1349–1364.
66. Project Min, E.A.L.S.S.C. (2018) Project MinE: study design and pilot analyses of a large-scale whole-genome sequencing study in amyotrophic lateral sclerosis. *Eur. J. Hum. Genet.*, **26**, 1537–1546.
67. Hashimoto,S., Sugiyama,T., Yamazaki,R., Nobuta,R. and Inada,T. (2020) Identification of a novel trigger complex that facilitates ribosome-associated quality control in mammalian cells. *Sci. Rep.*, **10**, 3422.
68. Radwan,M., Ang,C.S., Ormsby,A.R., Cox,D., Daly,J.C., Reid,G.E. and Hatters,D.M. (2020) Arginine in C9ORF72 dipolypeptides mediates promiscuous proteome binding and multiple modes of toxicity. *Mol. Cell. Proteomics*, **19**, 640–654.
69. Wang,F., Durfee,L.A. and Huibregtse,J.M. (2013) A Cotranslational Ubiquitination Pathway for Quality Control of Misfolded Proteins. *Mol. Cell*, **50**, 368–378.
70. Wang,L., Xu,Y., Rogers,H., Saidi,L., Noguchi,C.T., Li,H., Yewdell,J.W., Guydosh,N.R. and Ye,Y. (2020) UFMylation of RPL26 links translocation-associated quality control to endoplasmic reticulum protein homeostasis. *Cell Res.*, **30**, 5–20.
71. Matsuo,Y., Tesina,P., Nakajima,S., Mizuno,M., Endo,A., Buschauer,R., Cheng,J., Shounai,O., Ikeuchi,K., Saeki,Y. *et al.* (2020) RQT complex dissociates ribosomes collided on endogenous RQC substrate SDD1. *Nat. Struct. Mol. Biol.*, **27**, 323–332.
72. Hartmann,H., Hornburg,D., Czuppa,M., Bader,J., Michaelsen,M., Farny,D., Arzberger,T., Mann,M., Meissner,F. and Edbauer,D. (2018) Proteomics and C9orf72 neuropathology identify ribosomes as poly-GR/PR interactors driving toxicity. *Life Sci. Alliance*, **1**, e201800070.
73. Moens,T.G., Niccoli,T., Wilson,K.M., Atilano,M.L., Birsa,N., Gittings,L.M., Holbling,B.V., Dyson,M.C., Thoeng,A., Neeves,J. *et al.* (2019) C9orf72 arginine-rich dipeptide proteins interact with ribosomal proteins in vivo to induce a toxic translational arrest that is rescued by eIF1A. *Acta Neuropathol.*, **137**, 487–500.
74. Suzuki,H., Shibagaki,Y., Hattori,S. and Matsuoka,M. (2018) The proline–arginine repeat protein linked to C9-ALS/FTD causes neuronal toxicity by inhibiting the DEAD-box RNA helicase-mediated ribosome biogenesis. *Cell Death Dis.*, **9**, 975.
75. Andrade,N.S., Ramic,M., Esanov,R., Liu,W.J., Rybin,M.J., Gaidosh,G., Abdallah,A., Del'Olio,S., Huff,T.C., Chee,N.T. *et al.* (2020) Dipeptide repeat proteins inhibit homology-directed DNA double strand break repair in C9ORF72 ALS/FTD. *Mol. Neurodegener.*, **15**, 13.
76. Dafinca,R., Scaber,J., Ababneh,N., Lalic,T., Weir,G., Christian,H., Vowles,J., Douglas,A.G.L., Fletcher-Jones,A., Browne,C. *et al.* (2016) C9orf72 hexanucleotide expansions are associated with altered endoplasmic reticulum calcium homeostasis and stress granule formation in induced pluripotent stem cell-derived neurons from patients with amyotrophic lateral sclerosis and frontotemporal dementia. *Stem Cells*, **34**, 2063–2078.
77. Lopez-Gonzalez,R., Yang,D., Pribadi,M., Kim,T.S., Krishnan,G., Choi,S.Y., Lee,S., Coppola,G. and Gao,F.B. (2019) Partial inhibition of the overactivated Ku80-dependent DNA repair pathway rescues neurodegeneration in C9ORF72-ALS/FTD. *Proc. Natl. Acad. Sci. USA*, **116**, 9628–9633.
78. Meydan,S. and Guydosh,N.R. (2020) A cellular handbook for collided ribosomes: surveillance pathways and collision types. *Curr. Genet.*, **67**, 19–26.
79. Vind,A.C., Genzor,A.V. and Bekker-Jensen,S. (2020) Ribosomal stress-surveillance: three pathways is a magic number. *Nucleic Acids Res.*, **48**, 10648–10661.
80. Hickey,K.L., Dickson,K., Cogan,J.Z., Replogle,J.M., Schoof,M., D'Orazio,K.N., Sinha,N.K., Hussmann,J.A., Jost,M., Frost,A. *et al.* (2020) GIGYF2 and 4EHP inhibit translation initiation of defective messenger RNAs to Assist Ribosome-Associated Quality Control. *Mol. Cell*, **79**, 950–962.
81. Juszkiewicz,S., Slodkowicz,G., Lin,Z., Freire-Pritchett,P., Peak-Chew,S.Y. and Hegde,R.S. (2020) Ribosome collisions trigger cis-acting feedback inhibition of translation initiation. *Elife*, **9**, e60038.
82. Sinha,N.K., Ordureau,A., Best,K., Saba,J.A., Zinshteyn,B., Sundaramoorthy,E., Fulzele,A., Garshott,D.M., Denk,T., Thoms,M. *et al.* (2020) EDF1 coordinates cellular responses to ribosome collisions. *Elife*, **9**, e58828.
83. Weber,R., Chung,M.Y., Keskeny,C., Zinnall,U., Landthaler,M., Valkov,E., Izaurralde,E. and Igreja,C. (2020) 4EHP and GIGYF1/2 mediate Translation-Coupled messenger RNA decay. *Cell Rep.*, **33**, 108262.
84. Nissley,D.A., Vu,Q.V., Trovato,F., Ahmed,N., Jiang,Y., Li,M.S. and O'Brien,E.P. (2020) Electrostatic interactions govern extreme nascent protein ejection times from ribosomes and can delay ribosome recycling. *J. Am. Chem. Soc.*, **142**, 6103–6110.
85. Lu,J. and Deutsch,C. (2008) Electrostatics in the ribosomal tunnel modulate chain elongation rates. *J. Mol. Biol.*, **384**, 73–86.
86. Chu,J., Hong,N.A., Masuda,C.A., Jenkins,B.V., Nelms,K.A., Goodnow,C.C., Glynne,R.J., Wu,H., Masliah,E., Joazeiro,C.A.P. *et al.* (2009) A mouse forward genetics screen identifies LISTERIN as an E3 ubiquitin ligase involved in neurodegeneration. *Proc. Natl. Acad. Sci.*, **106**, 2097–2103.
87. Choe,Y.J., Park,S.H., Hassemer,T., Korner,R., Vincenz-Donnelly,L., Hayer-Hartl,M. and Hartl,F.U. (2016) Failure of RQC machinery causes protein aggregation and proteotoxic stress. *Nature*, **531**, 191–195.
88. Martin,P.B., Kigoshi-Tansho,Y., Sher,R.B., Ravenscroft,G., Stauffer,J.E., Kumar,R., Yonashiro,R., Muller,T., Griffith,C., Allen,W. *et al.* (2020) NEMF mutations that impair ribosome-associated quality control are associated with neuromuscular disease. *Nat. Commun.*, **11**, 4625.
89. Ishimura,R., Nagy,G., Dotu,I., Zhou,H., Yang,X.-L., Schimmel,P., Senju,S., Nishimura,Y., Chuang,J.H. and Ackerman,S.L. (2014) Ribosome stalling induced by mutation of a CNS-specific tRNA causes neurodegeneration. *Science*, **345**, 455–459.
90. Wu,Z., Tantray,I., Lim,J., Chen,S., Li,Y., Davis,Z., Sitron,C., Dong,J., Gispert,S., Auburger,G. *et al.* (2019) MISTERMINATE mechanistically links mitochondrial dysfunction with proteostasis failure. *Mol. Cell*, **75**, 835–848.

91. Ortega,J.A., Daley,E.L., Kour,S., Samani,M., Tellez,L., Smith,H.S., Hall,E.A., Esengul,Y.T., Tsai,Y.H., Gendron,T.F. *et al.* (2020) Nucleocytoplasmic Proteomic Analysis Uncovers eRF1 and Nonsense-Mediated Decay as Modifiers of ALS/FTD C9orf72 Toxicity. *Neuron*, **106**, 90–107.
92. Ju,S., Tardiff,D.F., Han,H., Divya,K., Zhong,Q., Maquat,L.E., Bosco,D.A., Hayward,L.J., Brown,R.H. Jr, Lindquist,S. *et al.* (2011) A yeast model of FUS/TLS-dependent cytotoxicity. *PLoS Biol.*, **9**, e1001052.
93. Armakola,M., Higgins,M.J., Figley,M.D., Barmada,S.J., Scarborough,E.A., Diaz,Z., Fang,X., Shorter,J., Krogan,N.J., Finkbeiner,S. *et al.* (2012) Inhibition of RNA lariat debranching enzyme suppresses TDP-43 toxicity in ALS disease models. *Nat. Genet.*, **44**, 1302–1309.
94. Barmada,S.J., Ju,S., Arjun,A., Batarse,A., Archbold,H.C., Peisach,D., Li,X., Zhang,Y., Tank,E.M.H., Qiu,H. *et al.* (2015) Amelioration of toxicity in neuronal models of amyotrophic lateral sclerosis by hUPF1. *Proc. Natl. Acad. Sci. USA*, **112**, 7821–7826.
95. Jackson,K.L., Dayton,R.D., Orchard,E.A., Ju,S., Ringe,D., Petsko,G.A., Maquat,L.E. and Klein,R.L. (2015) Preservation of forelimb function by UPF1 gene therapy in a rat model of TDP-43-induced motor paralysis. *Gene Ther.*, **22**, 20–28.
96. Li,S., Wu,Z., Tantray,I., Li,Y., Chen,S., Dong,J., Glynn,S., Vogel,H., Snyder,M. and Lu,B. (2020) Quality-control mechanisms targeting translationally stalled and C-terminally extended poly(GR) associated with ALS/FTD. *Proc. Natl. Acad. Sci. U.S.A.*, **117**, 25104–25115.